

A Nonlinear Finite Element Heterogeneous Multiscale Method for the Homogenization of Hyperelastic Solids and a Novel Staggered Two-Scale Solution Algorithm

Bernhard Eidel, Andreas Fischer, Ajinkya Gote

Heisenberg Group, Institute of Mechanics, Department Mechanical Engineering
Universität Siegen, 57068 Siegen, Paul-Bonatz-Str. 9-11, Germany
e-mail: bernhard.eidel@uni-siegen.de, phone: +49 271 740 2224, fax: +49 271 740 2436

Abstract

In this paper we address three aspects of nonlinear computational homogenization of elastic solids by two-scale finite element methods. First, we present a nonlinear formulation of the finite element heterogeneous multiscale method FE-HMM in a Lagrangean formulation that covers geometrical nonlinearity and, more generally, hyperelasticity. Second, we revise the standard solution algorithm of FE² which is a staggered scheme in terms of a nested loop embedding the full solution of the micro-problem into one macro-solution iteration step. We demonstrate that suchlike staggered scheme, which is typically realized by a nested two-level Newton algorithm, can safely and efficiently be replaced by direct alternations between micro- and macro iterations. The novel algorithmic structure is exemplarily detailed for the proposed nonlinear FE-HMM, its efficiency is substantiated by a considerable speed-up in numerical tests. Third, a-priori estimates of FE-HMM, which exist so far only for the fully linear elastic case in solid mechanics, are assessed in the regimes of nonlinear elasticity. The measured convergence rates agree fairly well with those of the fully linear regime.

Keywords: Heterogeneous multiscale method; Finite element method; Macro-to-micro modeling; Homogenization

1 Introduction

For the solution of homogenization problems, two-scale finite element methods like the FE²-method and the Finite Element Heterogeneous Multiscale Method FE-HMM combine in a favorable manner the needs for both accuracy and efficiency in that they sample the real microstructure in representative volume elements RVEs of confined size. By virtue of the equivalence of the coarse-scale energy density with the fine-scale energy density these methods stand on sound ground in physics, by virtue of the a priori estimates developed for FE-HMM, they are equipped with necessary ingredients in mathematics.

In spite of considerable achievements in the field, there is space for improvements; the present work addresses three of them.

1. **Nonlinear FE-HMM.** A nonlinear version of the Finite Element Heterogeneous Multiscale Method FE-HMM is developed for the homogenization of solids.
2. **A priori estimates.** An assessment of the a priori estimates of linear FE-HMM is carried out in the nonlinear regime of hyperelasticity.

3. **Solution algorithm.** The revision and improvement of the standard algorithmic structure of nonlinear two-scale finite element methods for homogenization like the FE² method and the present nonlinear FE-HMM.

These aims shall be motivated and put into perspective by a brief account of the state of the art.

1.1 Development of a nonlinear FE-HMM

FE-HMM formulations for problems in solid mechanics are so far restricted to linear problems, i.e. to linear elasticity in a geometrical linear setting; Abdulle [2006] presents a fully discrete convergence analysis taking into account the discretization errors at both micro and macro levels.

FE² and FE-HMM are equivalent methods, for a comparison see Eidel and Fischer [2018]; they are siblings (if not twins) having different parents. FE², an engineering mechanics offspring, is quite outgoing since its infancy and, unburdened from the necessity of delivering mathematical results on existence and uniqueness of solutions, has appreciated direct contact with nonlinear problems since its first appearance Michel et al. [1999], Miehe et al. [1999a], Miehe et al. [1999b], Feyel and Chaboche [2000], Kouznetsova et al. [2001]. FE-HMM as a method of mathematicians has grown up subject to the restriction, first prove, then apply; consequently its playground of applications was mostly in linear problems, comprehensive overviews are given in E et al. [2007], Abdulle [2009], Abdulle et al. [2012]. For the mathematical analysis of FE-HMM in the nonlinear regime of elliptic PDEs, results are sparse. Abdulle and Huber [2016] consider nonlinear monotone elliptic problems. For the same case Henning and Ohlberger [2015] derive a-posteriori error estimates for the L^2 -error between the HMM approximation and the solution of the macroscopic limit equation. Shirazi-Nejad and Wieners [2019] present an FE-HMM formulation for inelasticity that draws on the tangent moduli for stiffness-transfer and therein very much resembles the FE² method.

The present work proposes a nonlinear FE-HMM formulation for solid mechanics, which implies geometrical nonlinearity, either along with linear elasticity or nonlinear hyperelasticity. The extension to inelastic constitutive laws is a minor step following the perspective that inelasticity –in finite element numerics– can be understood as a type of nonlinear elasticity along with evolution equations for the inelastic deformation part treated as internal variables.

1.2 Test of the a priori estimates of linear FE-HMM for hyperelasticity

Error estimates are a necessary equipment of numerical methods to serve as reliable tools in science and engineering. By virtue of its foundation in mathematical homogenization by asymptotic expansion a priori estimates are available for FE-HMM; for the elliptic case in E et al. [2005], Ohlberger [2005], for the elliptic case of linear elasticity in a geometrical linear setting to Abdulle [2006], Abdulle [2009]. An assessment of the a priori estimates for various energetically consistent boundary conditions applied to the micro domain is presented in Fischer and Eidel [2019].

In the present work we assess the convergence of FE-HMM solutions in the nonlinear

regime of hyperelastic material behavior, although the estimates are derived for the setting of linear elasticity (generally, for linear elliptic PDEs). This will be carried out by a comparison with the linear case, which clarifies, whether the deviation from the estimates are caused by a lowered regularity of the boundary value problem or whether the deviation follows from the nonlinearities of the considered setting.

1.3 Speedup through modified algorithmic structure of two-scale FEM

In view of the considerable computational costs of two-scale FEM in homogenization there is a need for methodic advancements aiming at improved performance. For that aim several new and modified methods have been developed beyond parallelization.

Homogenization techniques based on Fast Fourier Transforms (FFT) were introduced in Moulinec and Suquet [1994], Moulinec and Suquet [1998], which are built on a Lippmann-Schwinger formulation Zeller and Dederichs [1973], Kröner [1971]; applicability and efficiency was demonstrated in Schneider et al. [2015], Schneider et al. [2017], and many more. Reduced basis methods and model order reduction exhibit considerable potential to speed up simulations; Yvonnet and He [2007] introduced a general (Galerkin) projection based reduced order model referred to as R3M where the reduced basis is obtained via snapshot proper orthogonal decomposition. Applications to nonlinear elasticity in Radermacher and Reese [2016], to homogenization problems in Soldner et al. [2017]. The derived reduced problems are low-dimensional and nonlinear. In an effort to reduce the computational complexity by a modified modeling Schröder et al. [2010] consider in FE^2 statistically similar representative volume elements (SSRVE) in order to replace the true microstructure in its full geometrical complexity by a simplified surrogate that resembles the original one by geometrical features as analyzed by different geometrical similarity measures. Domain-decomposition based on a FETI (finite element tearing and interconnect) have been proposed and successfully applied Klawonn and Rheinbach [2006], Klawonn and Rheinbach [2010].

The present work aims at speeding up computations through an improvement of the standard algorithmic concept of FE^2 . The discretized variational form of the balance of linear momentum both on the macro level and the micro level amount to systems of nonlinear algebraic equations, which are each typically but not necessarily solved by Newton's method. More important, the algorithmic solution framework is not monolithic, but exhibits a staggered structure, which provides a mutual exchange of coupling quantities (micro-to-macro: current micro stiffness and stress, macro-to-micro: current macro-deformation) between the macro problem and the micro problems.

The very standard of suchlike staggered scheme is realized by a nested loop embedding the full solution of the micro problems into one macro solution iteration step as sketched in the pseudocode of "Algorithm 1".

The attribute *standard* is set by a multitude of contributions to the field, Feyel and Chaboche [2000] p. 313, Kouznetsova et al. [2001] pp. 41,42, Miehe and Koch [2002] pp. 302,303, Miehe [2003] p. 574, Feyel [2003] p. 3236, Kouznetsova et al. [2004] p. 5532, for thermomechanical problems Özdemir et al. [2008] p. 606, Temizer and Wriggers [2008] p. 499, Schröder [2014] p. 8, for different coupling conditions at finite deformations Saeb et al. [2016] p. 20, for nonlinear monotone elliptic problems in FE-HMM Abdulle and Huber [2016] p. 966, Klawonn et al. [2019] p. 7, to name but a few.

Algorithm 1: nested (standard)

```

while macro residual < macro tolerance do
  | macro iteration;
  | while micro residual < micro tolerance do
  | | micro iteration;
  | end
end

```

In the present work a revision of this established scheme is carried out along with the proposal to replace it by an algorithm of direct alternations between micro and macro iterations as sketched in the pseudocode box "Algorithm 2".

Algorithm 2: alternating (novel)

```

while macro residual < macro tolerance do
  | macro iteration;
  | micro iteration;
end

```

The novel scheme, which was introduced in Eidel et al. [2018], is described in more detail in Sec. 5.2. Its properties and benefits in terms of accuracy, efficiency and stability with respect to large load step sizes are assessed in the example section 6.

The paper is organized along the route of the above aims.

2 Strong and variational forms

We consider a body \mathcal{B}_0 , a bounded subset of $\mathbb{R}^{n_{dim}}$, $n_{dim} = 2, 3$, with boundary $\partial\mathcal{B}_0 = \partial\mathcal{B}_{0D} \cup \partial\mathcal{B}_{0N}$ where $\partial\mathcal{B}_{0D}$ and $\partial\mathcal{B}_{0N}$ are disjoint sets. The closure of the body \mathcal{B} is denoted by $\bar{\mathcal{B}}$. The body undergoes deformation $\varphi : \Omega \rightarrow \mathbb{R}^{n_{dim}}$ with deformation gradient $\mathbf{F} = \partial_{\mathbf{X}}\varphi(\mathbf{X})$ and the Jacobian $J = \det\mathbf{F} > 0$, where \mathbf{X} is a material point in the reference configuration. The body is subject to body forces \mathbf{b} and surface tractions \mathbf{g} and in static equilibrium

$$\text{Div}[\mathbf{P}] + \rho \mathbf{b} = \mathbf{0} \tag{1}$$

in terms of the first Piola-Kirchhoff stress tensor \mathbf{P} , density ρ in the reference configuration, and body forces \mathbf{b} neglecting inertia terms.

Dirichlet and Neumann boundary conditions are prescribed by

$$\mathbf{u} = \hat{\mathbf{u}} \quad \text{on} \quad \partial\mathcal{B}_{0D} \quad \text{and} \quad \mathbf{P} \cdot \mathbf{N} = \mathbf{t} \quad \text{on} \quad \partial\mathcal{B}_{0N}. \tag{2}$$

The corresponding variational form reads

$$G := \int_{\mathcal{B}_0} (\text{Div}[\mathbf{P}] + \rho \mathbf{b}) \cdot \delta \mathbf{u} \, dV = 0, \tag{3}$$

with virtual displacements/test functions $\delta \mathbf{u}$ which can be transformed by $\text{Div}[\mathbf{P}^T \cdot \delta \mathbf{u}] - \mathbf{P} : \text{Grad}[\mathbf{P}^T \cdot \delta \mathbf{u}]$ into

$$G := \underbrace{\int_{\mathcal{B}_0} \mathbf{P} : \text{Grad}[\delta \mathbf{u}] \, dV}_{= G^{ext}} - \underbrace{\int_{\partial \mathcal{B}_{0N}} \mathbf{t} \cdot \delta \mathbf{u} \, dA - \int_{\mathcal{B}_0} \rho \mathbf{b} \cdot \delta \mathbf{u} \, dV}_{= G^{int}} = 0, \quad (4)$$

which has to hold for all $\delta \mathbf{u} \in \mathcal{V}$, where \mathcal{V} is the space of admissible displacements, i.e. virtual displacements that fulfill homogeneous Dirichlet boundary conditions

$$\mathcal{V} = \{\delta \mathbf{u}; \mathbf{u} \in H^1(\mathcal{B}_0)^{n_{dim}}, \mathbf{u}|_{\partial \mathcal{B}_{0D}} = \mathbf{0}\}. \quad (5)$$

With

$$\mathbf{P} : \text{Grad}[\delta \mathbf{u}] = \mathbf{S} : \mathbf{F}^T \cdot \text{Grad}[\delta \mathbf{u}] = \mathbf{S} : \frac{1}{2}(\mathbf{F}^T \cdot \delta \mathbf{F} + \delta \mathbf{F}^T \cdot \mathbf{F}) = \mathbf{S} : \delta \mathbf{E} \quad (6)$$

the virtual work can be equally expressed by the second Piola Kirchhoff stress tensor \mathbf{S} and the Green-Lagrange strain tensor \mathbf{E}

$$G := \int_{\mathcal{B}_0} \frac{1}{2} \mathbf{S} : \delta \mathbf{E} \, dV - \int_{\partial \mathcal{B}_{0N}} \mathbf{t} \cdot \delta \mathbf{u} \, dA - \int_{\mathcal{B}_0} \rho \mathbf{b} \cdot \delta \mathbf{u} \, dV = 0. \quad (7)$$

2.1 Characteristics and conditions for computational homogenization

For the solution of the BVP in its strong form or variational form, constitutive laws must be defined in the domain \mathcal{B}_0 for which we assume matter to be heterogeneous in its properties, such that the solution to the BVP shall be found through homogenization. For the application of homogenization in terms of computational micro-macro transitions several conditions must be fulfilled, which partly refer to the characteristics of the very problem, partly to mathematical homogenization, and partly to the properties of the solution method. Consequently, the following assumptions are made:

- **Scale separation.** A prerequisite of homogenization is that the characteristic length scale of microstructural features must be *considerably* smaller than the characteristic length scale on the macro scale¹ $L_{mac} \gg L_{mic}$. The deeper root of this requirement is mathematical homogenization, since the separation of length scales is necessary for the corresponding separation of variables in homogenization theory, Bensoussan et al. [1976], Sanchez-Palencia [1980], Guedes and Kikuchi [1990], Allaire [1992], Cioranescu and Donato [1999].
- **Sampling domains.** For the microstructure on the fine scale a statistically representative volume element RVE is available, Hill [1963], Ostoja-Starzewski [2006], Sab [1992], Drugan and Willis [1996].
- **Constitutive equations.** The type of constitutive law and its parameters are available for matter in the RVE, for its constituents (grains, phases, etc.) and interfaces, but not on the macro scale in terms of effective laws and their parameters.

¹We use macro/coarse scale and micro-/fine-scale each as synonyms.

- **Coupling conditions.** The coupling conditions cover a kinematical and an energetic aspect. The equivalence of energy densities of the coarse scale with the fine scale is the cornerstone of homogenization, Hill [1963], Mandel [1971], Hill [1972], E and Engquist [2003]. The proper kinematical embedding of the micro domain into the macro domain with respect to deformation and (Dirichlet and Neumann) boundary conditions on the RVE follows from energy equivalence. Since they are not unique, additional modeling assumptions must be made.
- **Scale interaction and data transfer.** The conditions for these two items follow from the above items Constitutive equations and Coupling conditions. The macro BVP is the driver of the micro BVP through deformation in the coupling conditions, the top-down direction of data transfer. Since constitutive equations with parameters are a priori exclusively available on the micro scale, the numerical solution of the macro BVP requires stiffness and stress from the fine scale, the bottom-up direction of data transfer.

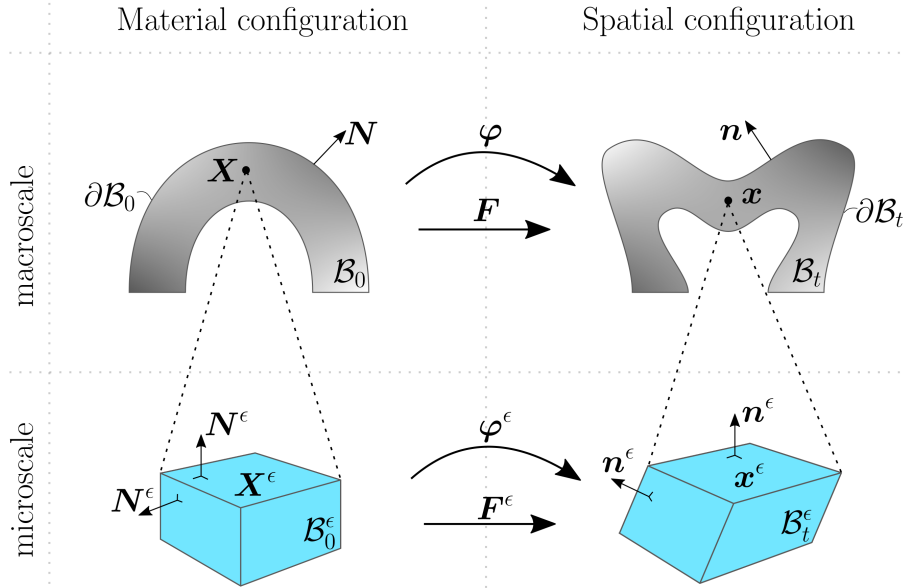


Figure 1: Homogenization: The general setting of micro-macro transition in material and spatial configurations.

While balance laws are scale invariant and therefore are known and apply for the macro as well as the micro scale, the effective constitutive law along with its parameters is not known for the macro scale but exclusively for the micro scale, here in terms of the hyperelasticity relations

$$\mathbf{P}^\epsilon = \frac{\partial \psi^\epsilon}{\partial \mathbf{F}^\epsilon}, \quad \mathbb{A}^\epsilon = \frac{\partial^2 \psi^\epsilon}{\partial \mathbf{F}^\epsilon \partial \mathbf{F}^\epsilon}, \quad \mathbf{S}^\epsilon = \mathbf{F}^{\epsilon-1} \mathbf{P}^\epsilon, \quad (8)$$

where we indicate microscale quantities by ϵ as borrowed from mathematical homogenization, where it refers to the (periodic) cell size.

The Hill-Mandel energy equivalence principle is formulated as an equivalence of stress power in terms of the first Piola-Kirchhoff stress tensor and the material time derivative

of the work-conjugate deformation gradient \mathbf{F}

$$\mathbf{P} : \dot{\mathbf{F}} = \frac{1}{V} \int_{\mathcal{B}_0} \mathbf{P}^\epsilon : \dot{\mathbf{F}}^\epsilon dV, \quad (9)$$

where their averages are defined according to

$$\mathbf{P} = \langle \mathbf{P}^\epsilon \rangle_0, \quad \mathbf{F} = \langle \mathbf{F}^\epsilon \rangle_0, \quad \text{with} \quad \langle \{\bullet\} \rangle_0 = \frac{1}{V_0} \int_{V_0} \{\bullet\} dV. \quad (10)$$

The volume average for the deformation gradient according to (10)₂ is only valid for cases without hollow spaces in the microstructure like voids, cracks, or for cellular materials, since it holds

$$\mathbf{F} := \frac{1}{V} \int_{\partial \mathcal{B}_0} \mathbf{x} \otimes \mathbf{N} dA = \frac{1}{V} \left[\int_{\mathcal{B}_0} \mathbf{F} dV - \int_{|\circ|} \mathbf{x} \otimes \mathbf{N} dA \right], \quad (11)$$

where \mathbf{x} is the position vector of a point in \mathcal{B}_0 , \mathbf{N} is the normal on $\partial \mathcal{B}_0$ and $|\circ|$ represents the boundaries of hollow space.

Since the present FE-HMM framework is formulated in the reference configuration with the work conjugate pair of the second Piola-Kirchhoff stress and the Green-Lagrange strain tensor, the macro average stress must be consistent with (10) in (9), it holds

$$\mathbf{S} = \langle \mathbf{F}^\epsilon \rangle_0^{-1} \langle \mathbf{P}^\epsilon \rangle_0. \quad (12)$$

An averaged macro stress according to $\mathbf{S}^* := \langle \mathbf{S}^\epsilon \rangle_0$ is not consistent with (10) since $\mathbf{S} \neq \mathbf{S}^*$.

A framework for equivalence relationships for finite strain multi-scale solid constitutive models based on the volume averaging of the microscopic stress and deformation gradient fields over a representative volume element (RVE) is presented in de Souza Neto and Feijóo [2008]. Based on a purely kinematically-based variational framework they derive sufficient conditions under which the volume average of the microscopic first Piola-Kirchhoff stress over the material configuration of the RVE is mechanically equivalent to the average of the microscopic Cauchy stress field over the spatial configuration.

Similar to the present work, the weak form in \mathbf{S} and \mathbf{E} in the context of FE² is chosen in Grytz and Meschke [2008] and van Dijk [2016].

3 The Heterogeneous Multiscale Finite Element Method

A nonlinear version of FE-HMM is derived for the application to geometrical nonlinear problems in solid mechanics based on linear elastic or (nonlinear) hyperelastic constitutive laws. In the example section 6 we will consider Neo-Hookean-type hyperelasticity. While the majority of homogenization schemes is formulated in reference configuration in terms of \mathbf{P} and \mathbf{F} , we employ the work-conjugate pair \mathbf{S} and \mathbf{E} .

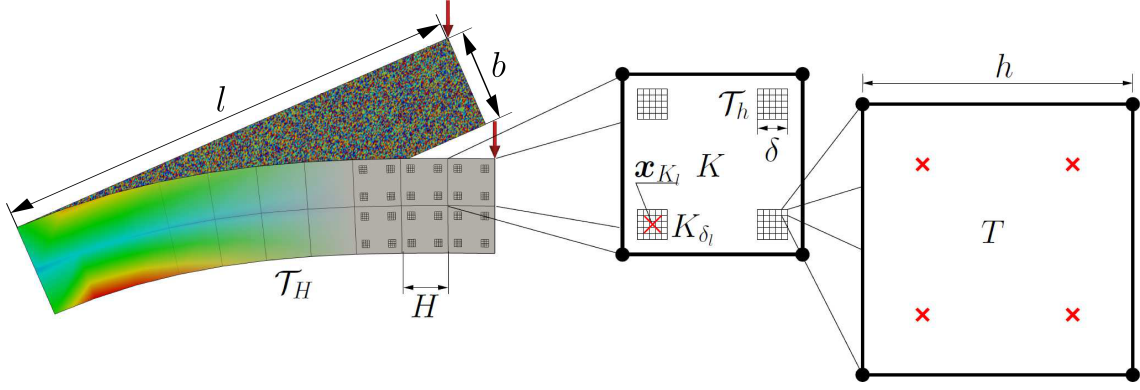


Figure 2: Micro-macro transition of FE-HMM: The triangulation of the macro problem \mathcal{T}_H results in finite elements K of size H . Micro sampling domains of characteristic length δ in triangulation \mathcal{T}_h into elements T of size h are attached to the macro quadrature points $\mathbf{x}_{K_{\delta_l}}$ of K , hence spanning the sampling domain $K_{\delta_l} = \mathbf{x}_{K_{\delta_l}} + \delta [-1/2, +1/2]^{n_{dim}}$, $\delta \geq \epsilon$, centered at quadrature points (qp), $l = 1, \dots, N_{qp}$. The separation of length scales imposes the condition $\{l, b\} \gg \epsilon$.

3.1 Discretization and linearization of the variational form

Here we consider the piecewise linear continuous FEM in macro and micro space, respectively.

We define a macro finite element space as

$$\mathcal{S}_{\partial\mathcal{B}_{0D}}^p(\mathcal{B}_0, \mathcal{T}_H) = \{ \mathbf{u}^H \in H^1(\mathcal{B}_0)^{n_{dim}}; \mathbf{u}^H|_{\partial\mathcal{B}_{0D}} = \mathbf{0}; \mathbf{u}^H|_K \in \mathcal{P}^p(K)^{n_{dim}}, \forall K \in \mathcal{T}_H \} \quad (13)$$

where \mathcal{P}^p is the space of (in the present work: linear, $p = 1$) polynomials on the element K , \mathcal{T}_H the (quasi-uniform) triangulation of $\mathcal{B}_0 \subset \mathbb{R}^{n_{dim}}$. The space $\mathcal{S}_{\partial\mathcal{B}_{0D}}^p$ is a subspace of \mathcal{V} defined in (5). The characteristic element size on the macro scale H (Fig. 2) refers in index or superscript to macro scale quantities in the discretized setting, the characteristic micro element size h analogously marks micro scale quantities of the discrete case.

For the solution of the macro scale BVP we use the two-scale FEM framework of the FE-HMM, as originally proposed in E and Engquist [2003] and analyzed for elliptic PDEs in E et al. [2005].

The macro solution of the FE-HMM is given by the following variational form:

Find $\mathbf{u}^H \in \mathcal{S}_{\partial\mathcal{B}_{0D}}(\mathcal{B}_0, \mathcal{T}_H)$ such that

$$G^H(\mathbf{u}^H, \delta\mathbf{u}^H) = \int_{\mathcal{B}_0} \frac{1}{2} \mathbf{S} : \delta\mathbf{E} \, dV - \int_{\partial\mathcal{B}_{0N}} \mathbf{t} \cdot \delta\mathbf{u}^H \, dA - \int_{\mathcal{B}_0} \mathbf{b} \cdot \delta\mathbf{u}^H \, dV \quad \forall \delta\mathbf{u}^H \in \mathcal{S}_{\partial\mathcal{B}_{0D}}(\mathcal{B}_0, \mathcal{T}_H). \quad (14)$$

Standard finite element shape functions N_I are used for the interpolation

$$\mathbf{u}^H = \sum_{I=1}^{N_{node}} N_I \mathbf{d}_I^H, \quad \mathbf{u}^h = \sum_{I=1}^{N_{node}} N_I \mathbf{d}_I^h, \quad (15)$$

of nodal displacement vectors $\mathbf{d}_I^H, \mathbf{d}_I^h$, where N_{node} is the number of nodes per element. Virtual displacements $\delta\mathbf{u}^H$ and $\delta\mathbf{u}^h$ are equally obtained through interpolation of nodal

values $\delta \mathbf{d}_I^H$ and $\delta \mathbf{d}_I^h$, respectively. Consequently, we obtain for G^H in (14)

$$G^H(\mathbf{u}^H, \delta \mathbf{u}^H) = \sum_{I=1}^{N_{node}} (\delta \mathbf{d}_I^H)^T \mathbf{f}_I^H \quad \text{with} \quad \mathbf{f}_I^H = \mathbf{f}_I^{int,H} - \mathbf{f}_I^{ext,H} \quad (16)$$

and for the analogously defined G^h on the micro domain

$$G^h(\mathbf{u}^h, \delta \mathbf{u}^h) = \sum_{I=1}^{N_{node}} (\delta \mathbf{d}_I^h)^T \mathbf{f}_I^h \quad \text{with} \quad \mathbf{f}_I^h = \mathbf{f}_I^{int,h} - \mathbf{f}_I^{ext,h}. \quad (17)$$

The internal and external nodal force vectors are defined for node I of macro element K with volume $|K|$ and surface ∂K and for node I of micro element T with volume $|T|$ and surface ∂T

$$\mathbf{f}_I^{int,H} = \int_{|K|} \mathbf{B}_I^T \mathbf{S} \, dV, \quad \mathbf{f}_I^{int,h} = \int_{|T|} \mathbf{B}_I^T \mathbf{S}^h \, dV \quad (18)$$

$$\mathbf{f}_I^{ext,H} = \int_{\partial K} N_I \bar{\mathbf{t}} \, dA, \quad \mathbf{f}_I^{ext,h} = \int_{\partial T} N_I \mathbf{t} \, dA. \quad (19)$$

For the computation of $\mathbf{f}_I^{int,H}$ on the macro domain the second Piola-Kirchhoff stress \mathbf{S} is obtained according to (12), hence, along with our notation for the discretized case, by

$$\mathbf{S} = \langle \mathbf{F}^h \rangle_0^{-1} \langle \mathbf{P}^h \rangle_0. \quad (20)$$

3.2 The micro-to-macro stiffness transfer and assembly

Since G^H is nonlinear in \mathbf{u}^H , it is linearized at the current macro displacement state \mathbf{u}^H

$$\text{Lin} [G^H(\mathbf{u}^H, \delta \mathbf{u}^H)] = G^H(\mathbf{u}^H, \delta \mathbf{u}^H) + DG^H(\mathbf{u}^H, \delta \mathbf{u}^H) \cdot \Delta \mathbf{u}^H = 0. \quad (21)$$

The first term $G^H(\mathbf{u}^H, \delta \mathbf{u}^H)$ is the evaluation of G^H for the current macro displacement field, the second term is the linearization of G^H in the direction of the incremental macro displacements $\Delta \mathbf{u}^H$ (a Directional- or Gateaux-derivative).

In analogy to the linear case, the key step of nonlinear FE-HMM is to approximate in the numerical quadrature of (22) the macro values at the quadrature points by the volume-averaged integral of micro scale quantities according to (23)

$$\begin{aligned} DG^H(\mathbf{u}^H, \delta \mathbf{u}^H) \cdot \Delta \mathbf{u}^H &= \sum_{K \in \mathcal{T}_H} \sum_{l=1}^{N_{qp}} \omega_{K\delta_l} [\delta \mathbf{E} : \mathbb{C}_T : \Delta \mathbf{E} + \mathbf{S} : \Delta \delta \mathbf{E}] \, dV \quad (22) \\ &\approx \sum_{K \in \mathcal{T}_H} \sum_{l=1}^{N_{qp}} \omega_{K\delta_l} \left[\frac{1}{|K_{\delta_l}|} \int_{K_{\delta_l}} [\delta \mathbf{E}^h : \mathbb{C}_T^\epsilon : \Delta \mathbf{E}^h + \mathbf{S}^h : \Delta \delta \mathbf{E}^h] \, dV \right] \quad (23) \end{aligned}$$

The approximation reflects that the constitutive law in terms of the free energy function $\psi^0(\mathbf{x})$, and the derived quantities of stress \mathbf{S} and the tangent \mathbb{C}_T are not known.

The micro solution \mathbf{u}^h and derived quantities \mathbf{E}^h , \mathbb{C}_T^ϵ and \mathbf{S}^h are obtained

- on micro sampling domains $K_{\delta_l} = \mathbf{x}_{K_{\delta_l}} + \delta [-1/2, +1/2]^{n_{dim}}$, $\delta \geq \epsilon$, volume $|K_{\delta_l}|$
- centered at quadrature points $\mathbf{x}_{K_{\delta_l}}$ of K , $l = 1, \dots, N_{qp}$ with weights $\omega_{K_{\delta_l}}$,

for a visualization see Fig. 2. The micro sampling domains render the additive contribution to the tangential stiffness matrix of the macro finite element.

The approximation in numerical quadrature is consistent with the Hill-Mandel postulate of energy equivalence. It is, however, not sufficient. Since the pointwise macroscopic energy density is replaced by microscopic energy density in a volume, boundary conditions consistent to the postulate must be chosen.

The macro element tangential stiffness matrix contribution $\mathbf{k}_{T,IJ}^H$ for nodes I and J of element K are obtained –in analogy to the linear case– by inserting finite element shape functions into (22), hence $\delta \mathbf{u}^H(\mathbf{N}_I)$ and $\Delta \mathbf{u}^h(\mathbf{N}_J)$, which results in²

$$\mathbf{k}_{T,IJ,K}^H = \text{DG}^H(\mathbf{u}^H, \delta \mathbf{u}^H(\mathbf{N}_J)) \cdot \Delta \mathbf{u}^H(\mathbf{N}_I) \quad (24)$$

$$= \sum_{l=1}^{N_{qp}} \frac{\omega_{K_{\delta_l}}}{|K_{\delta_l}|} (\mathbf{D}^{h(I)})^T \mathbf{K}_{T,K_{\delta_l}}^h \mathbf{D}^{h(J)}, \quad (25)$$

$$\text{where } \mathbf{D}^{h(I)} = (\mathbf{D}^{h(I,x_1)} | \mathbf{D}^{h(I,x_2)} | \mathbf{D}^{h(I,x_3)}) \quad \text{for } n_{dim} = 3, \quad (26)$$

$$\mathbf{k}_{T,K}^H = \sum_{l=1}^{N_{qp}} \frac{\omega_{K_{\delta_l}}}{|K_{\delta_l}|} \mathbf{T}_{K_{\delta_l}}^T \mathbf{K}_{T,K_{\delta_l}}^h \mathbf{T}_{K_{\delta_l}}, \quad (27)$$

$$\text{where } \mathbf{T}_{K_{\delta_l}} = \left[\left[[\mathbf{D}^{h(I,x_i)}]_{i=1,\dots,n_{dim}} \right]_{I=1,\dots,N_{node}} \right]. \quad (28)$$

The assembly of the global micro stiffness matrix implies the arrangement of $\mathbf{D}^{h(I)}$ in different columns for $I = 1, \dots, N_{node}$, which results in the transformation matrix $\mathbf{T}_{K_{\delta_l}}$.

With M_{mic} for the number of nodes in the micro domain, and N_{node} for the number of elements on a macro element, it can be easily verified that the matrix dimensions of $\mathbf{T}_{K_{\delta_l}} \in \mathbb{R}^{(M_{mic} \cdot n_{dim}) \times (N_{node} \cdot n_{dim})}$, $\mathbf{K}_{T,K_{\delta_l}}^h \in \mathbb{R}^{(M_{mic} \cdot n_{dim}) \times (M_{mic} \cdot n_{dim})}$, and of $\mathbf{k}_{T,K}^H \in \mathbb{R}^{(N_{node} \cdot n_{dim}) \times (N_{node} \cdot n_{dim})}$ are consistently used in (27), and that $\mathbf{T}_{K_{\delta_l}}$ is an operator of micro-to-macro stiffness transfer and dimensional compression.

The single columns of this transformation matrix contain dimensionless displacements of the micro nodes following from macro unit displacement states in terms of shape functions. The superscript (I, x_i) encodes the unit displacement state at macro node I , $I = 1, \dots, N_{node}$ in the direction of x_i , $i = 1, \dots, n_{dim}$.

The transformation matrix and its derivation provide the information on how to carry out the computations for its entries; first, on the driver of the micro problem in terms of shape functions as described, second, on the corresponding solutions $\mathbf{d}^{h(I,x_i)}$, which build up $\mathbf{T}_{K_{\delta_l}}$. These two characteristics are not sufficient to properly solve the microproblem. The missing links are the coupling conditions, cf. Sec. 2.1.

- **Energetically consistent BCs.** They must be applied to the micro domain to comply (the Hill-Mandel postulate of) the micro-macro energy equivalence. The

²Here and in the following small letters (for stiffness matrices \mathbf{k} , force vectors \mathbf{f} , displacements \mathbf{d}) refer to the element level, capital letters to global, assembled quantities, which is applied for micro scale (h) and macro scale quantities (H).

most frequently used BCs are periodic (PBC), linear displacement or kinematically uniform BCs (KUBC/Dirichlet), and constant traction (Neumann) BCs.

- **Order of computational homogenization.** If the macro deformation imparted on the micro domain is homogeneous, the micro problem resembles the unit cell problem of (asymptotic) mathematical homogenization, which is the foundation of FE-HMM. In computational mechanics this setting is frequently referred to as first order computational homogenization. For that aim the macro displacements \mathbf{u}^H are linearized at quadrature points $\mathbf{x}_{K_{\delta_l}}$ according to

$$\mathbf{u}_{lin,K_{\delta_l}}^H = \mathbf{u}^H(\mathbf{x}_{K_{\delta_l}}) + (\mathbf{x} - \mathbf{x}_{K_{\delta_l}}) \cdot \nabla \mathbf{u}^H(\mathbf{x}_{K_{\delta_l}}). \quad (29)$$

With these coupling conditions the embedding of the micro problem into the macro continuum is defined and the micro problem can be solved. The task is cast into a saddle-point problem with the corresponding Lagrange-functional to be minimized.

For the micro problem driven by the linearized macroscopic unit displacement states (I, x_i) and thereby subject to energetically consistent BC, solve

$$\mathcal{L}(\mathbf{D}^{h(I,x_i)}, \boldsymbol{\Lambda}^{(I,x_i)}) = \frac{1}{2} \mathbf{D}^{h(I,x_i)T} \mathbf{K}_T^h \mathbf{D}^{h(I,x_i)} + \boldsymbol{\Lambda}^{(I,x_i)T} \mathbf{G} \left(\mathbf{D}^{h(I,x_i)} - \bar{\mathbf{d}}^{H(I,x_i)} \right) \rightarrow \min. \quad (30)$$

where³ $\bar{\mathbf{d}}^{H(I,x_i)}$ is the prescribed nodal displacement vector that follows from linearization in (29), and where the nodal constraints are encoded in matrix \mathbf{G} . For convenience we have dropped the index of \mathbf{K}_T^h but keep in mind that it refers to a micro problem at macro quadrature point K_{δ_l} . The first variation of \mathcal{L} with respect to both $\mathbf{D}^{h(I,x_i)}$ and $\boldsymbol{\Lambda}^{(I,x_i)}$ results in the set of linear equations to be solved for $I = 1, \dots, N_{Node}$, $i = 1, \dots, n_{dim}$:

$$\begin{bmatrix} \mathbf{K}_T^h & \mathbf{G}^T \\ \mathbf{G} & \mathbf{0} \end{bmatrix} \begin{bmatrix} \mathbf{D}^{h(I,x_i)} \\ \boldsymbol{\Lambda}^{(I,x_i)} \end{bmatrix} = \begin{bmatrix} \mathbf{0} \\ \mathbf{G} \bar{\mathbf{d}}^{H(I,x_i)} \end{bmatrix}, \quad (31)$$

where for PBC condition $\mathbf{G}^T \boldsymbol{\Lambda}^{(I,x_i)} = \mathbf{0}$ is fulfilled by the periodic displacements and antiperiodic tractions.

The solution vector contains the dimensionless micro displacements $\mathbf{D}^{h(I,x_i)}$, and the Lagrange multipliers $\boldsymbol{\Lambda}^{(I,x_i)}$ enforce the coupling condition. With $\mathbf{D}^{h(I,x_i)}$ the transformation matrix $\mathbf{T}_{K_{\delta_l}}$ and thereby the macro element stiffness matrix can be built as described by (27) and (28). Assembling the macro scale element contributions results in the global system of equations

$$\mathbf{A} \sum_{e=1}^{num_{ele}} \sum_{I=1}^{N_{node}} \sum_{J=1}^{N_{node}} (\delta \mathbf{d}_I^H)^T (\mathbf{k}_{T,IJ}^H \Delta \mathbf{d}_J^H + \mathbf{f}_I^H) = 0. \quad (32)$$

For PBC it holds for node p and its counterpart q at opposite edges (for $n_{dim} = 2$) and at opposite faces (for $n_{dim} = 3$) of a micro domain K_{δ_l} the constraint condition with $\mathbf{u}_{lin,K_{\delta_l}}^H$ according to (29)

$$\left(\mathbf{u}_{K_{\delta_l}}^h - \mathbf{u}_{lin,K_{\delta_l}}^H \right) (p) = \left(\mathbf{u}_{K_{\delta_l}}^h - \mathbf{u}_{lin,K_{\delta_l}}^H \right) (q) \quad (33)$$

$$\mathbf{G} \left(\mathbf{D}_{K_{\delta_l}}^h - \bar{\mathbf{d}}_{K_{\delta_l}}^H \right) = \mathbf{0}, \quad (34)$$

³The basis of the macro element quantity $\bar{\mathbf{d}}^H$ is that one of the micro space; therefore and to avoid notational confusion with assembled macro displacements, we employ small letter \mathbf{d} .

where (34) is the Lagrange multiplier counterpart, in which matrix \mathbf{G} encodes both the macro-micro coupling condition of homogeneous deformation mediated by $\bar{\mathbf{d}}_{K\delta_l}^H$ and the non-redundant periodic coupling conditions for partner nodes p, q on the micro domain boundary.

Notice that the micro problem and its solution in Sec. 3.2 merely serves the purpose of building the stiffness carrier \mathbf{T}_K . For the solution of the macro problem (i) macro stress from averaged micro stress $\mathbf{S} = \langle \mathbf{S}^h \rangle$ and (ii) macro stiffness \mathbf{k}_T^H from \mathbf{K}_T^h must be available, namely for the micro state fulfilling the weak form of balance of linear momentum. For that purpose the micro problem is to be solved which is described in the following Sec. 3.3.

3.3 The microproblem and its solution

The micro problem is solved on the RVE of each macro quadrature point $K_{\delta_l}, l = 1, \dots, n_{qp}$ in all finite elements K of the macro triangulation \mathcal{T}^H .

The solution of the nonlinear system of equations on the micro domain from (17) requires the linearization at the current micro displacement state \mathbf{u}^h

$$\text{Lin} [G^h(\mathbf{u}^h, \delta\mathbf{u}^h)] = G^h(\mathbf{u}^h, \delta\mathbf{u}^h) + DG^h(\mathbf{u}^h, \delta\mathbf{u}^h) \cdot \Delta\mathbf{u}^h = 0, \quad (35)$$

with the definitions already introduced in the context of the linearization of G^H .

The approximation of $DG \cdot \Delta\mathbf{u}$ is given by

$$DG^h(\mathbf{u}^h, \delta\mathbf{u}^h) \cdot \Delta\mathbf{u}^h = \int_T (\delta\mathbf{E} : \mathbb{C}_T^\varepsilon : \Delta\mathbf{E} + \mathbf{S} : \Delta\delta\mathbf{E}) \, dV. \quad (36)$$

Inserting the approximations into the framework of the finite element method leads to

$$DG^h(\mathbf{u}^h, \delta\mathbf{u}^h) \cdot \Delta\mathbf{u}^h = \sum_{I=1}^{N_{node}} \sum_{K=1}^{N_{node}} (\delta\mathbf{d}_I^h)^T \underbrace{\int_T (\mathbf{B}_I^T \mathbb{C}_T^\varepsilon \mathbf{B}_K + \hat{\mathbf{G}}_{IK}) \, dV}_{=: \mathbf{k}_{T,IK}^h} \Delta\mathbf{d}_K^h, \quad (37)$$

with the tangential element stiffness matrix contribution of nodes I and K and the initial stress matrix $\hat{\mathbf{G}}_{IK}$ reflecting the contribution of the current stress state to the stiffness of a deformed structure

$$\hat{\mathbf{G}}_{IK} = \hat{S}_{IK} \mathbf{1} \quad \text{with} \quad (38)$$

$$\begin{aligned} \hat{S}_{IK} = & S^{11} N_{I,1} N_{K,1} + S^{22} N_{I,2} N_{K,2} + S^{33} N_{I,3} N_{K,3} + S^{12} (N_{I,1} N_{K,2} + N_{I,2} N_{K,1}) + \\ & S^{13} (N_{I,1} N_{K,3} + N_{I,3} N_{K,1}) + S^{23} (N_{I,2} N_{K,3} + N_{I,3} N_{K,2}). \end{aligned} \quad (39)$$

The corresponding global finite element approximation on the micro scale is obtained by assembling the contributions of all micro finite elements (number: num_{ele})

$$\mathbf{A} \sum_{e=1}^{num_{ele}} \sum_{I=1}^{N_{node}} \sum_{K=1}^{N_{node}} (\delta\mathbf{d}_I^h)^T (\mathbf{k}_{T,IK}^h \Delta\mathbf{d}_K^h + \mathbf{f}_I^h) = 0. \quad (40)$$

The assembled system of equations (40) is subject to the coupling conditions, hence

$$\mathbf{K}_T^h \Delta \mathbf{D}^h + \mathbf{F}^h = \mathbf{0} \quad \text{subject to} \quad \mathbf{G} \left(\Delta \mathbf{D}^h - \bar{\mathbf{d}}^H \right) = \mathbf{0}. \quad (41)$$

In the incremental setting of linearized equations along with the constraint matrix \mathbf{G} , the constraint for energetically consistent BCs is written in terms of the yet unknown micro displacement increment $\Delta \mathbf{D}^h$ and the macroscopic displacements $\bar{\mathbf{d}}^H$ imposed on the RVE boundary nodes to realize the required homogeneous deformation.

For the solution of (41) a Lagrange-functional is constructed which is to be minimized.

$$\mathcal{L}(\Delta \mathbf{D}^h, \Delta \boldsymbol{\Lambda}^h) = \frac{1}{2} \Delta \mathbf{D}^{hT} \mathbf{K}_T^h \Delta \mathbf{D}^h + \mathbf{F}^{hT} \Delta \mathbf{D}^h + \Delta \boldsymbol{\Lambda}^{hT} \mathbf{G} \left(\Delta \mathbf{D}^h - \bar{\mathbf{d}}^H \right) \longrightarrow \min. \quad (42)$$

The partial derivative of \mathcal{L} with respect to $\Delta \mathbf{D}^h$ and with respect to $\Delta \boldsymbol{\Lambda}^h$ yield the stationarity conditions

$$\begin{bmatrix} \mathbf{K}_T^h & \mathbf{G}^T \\ \mathbf{G} & \mathbf{0} \end{bmatrix} \begin{bmatrix} \Delta \mathbf{D}^h \\ \Delta \boldsymbol{\Lambda}^h \end{bmatrix} = \begin{bmatrix} -\mathbf{F}^h \\ \mathbf{G} \bar{\mathbf{d}}^H \end{bmatrix}. \quad (43)$$

Therein, the first set of equations

$$\mathbf{K}_T^h \Delta \mathbf{D}^h = \underbrace{-\mathbf{F}^h - \mathbf{G}^T \Delta \boldsymbol{\Lambda}^h}_{=: -\mathbf{R}^h} \quad (44)$$

corresponds to (41), the term $\mathbf{G}^T \Delta \boldsymbol{\Lambda}^h$ describes the change of the external node forces (Lagrange multipliers enforcing the coupling), which, together with the internal force vector \mathbf{F}^h , render the residual \mathbf{R}^h . In the case of PBC the change of these external node forces is not considered in the linearization, since $\mathbf{G}^T \Delta \boldsymbol{\Lambda}^h = \mathbf{0}$ is fulfilled by periodic displacements and antiperiodic tractions.

The solution of (43) yields the updates

$$\mathbf{D}^h \longleftarrow \mathbf{D}^h + \Delta \mathbf{D}^h, \quad (45)$$

$$\boldsymbol{\Lambda}^h \longleftarrow \boldsymbol{\Lambda}^h + \Delta \boldsymbol{\Lambda}^h. \quad (46)$$

Iterations along with updates stop for sufficiently small residuals. Then the computation of the micro-to-macro stiffness transfer by means of the current tangential stiffness matrix and by means of the current stress transfer is carried out.

The application of energetically consistent BCs fulfilling the Hill-Mandel condition in the FE-HMM framework are analyzed in Fischer and Eidel [2019] for linear elasticity along with convergence and error analysis, for finite deformations see Saeb et al. [2016].

Remarks

The differences in the Lagrange functionals of (30) in comparison to (42) reflects their different purpose; (42) is constructed for the continuation of a Newton iteration by linearized equations in (43), whereas (30) is constructed from truly linear equations; for a state fulfilling the balance equations after having solved the nonlinear set of algebraic equations, it is now purely the task of the micro-to-macro stiffness transfer. The stiffness

transfer coincides with that one in linear homogenization. For the linear case the tangential stiffness matrix boils down to the deformation- and stress-independent stiffness matrix, Eidel and Fischer [2016], Eidel and Fischer [2018].

The FE² method realizes the micro-macro stiffness transfer in terms of the homogenized elasticity tensor/tangent moduli, which are obtained by means of the micro stiffness matrix. FE-HMM in contrast directly draws on the micro stiffness matrices as described.

4 A priori error estimates

By virtue of its foundation in mathematical homogenization by asymptotic expansion a priori estimates are available for FE-HMM; for the elliptic case in E et al. [2005], Ohlberger [2005], for the elliptic case of linear elasticity in a geometrical linear setting to Abdulle [2006], Abdulle [2009].

The total FE-HMM error can be decomposed into three parts

$$\|\mathbf{u}^0 - \mathbf{u}^H\| \leq \underbrace{\|\mathbf{u}^0 - \mathbf{u}^{0,H}\|}_{e_{mac}} + \underbrace{\|\mathbf{u}^{0,H} - \tilde{\mathbf{u}}^H\|}_{e_{mod}} + \underbrace{\|\tilde{\mathbf{u}}^H - \mathbf{u}^H\|}_{e_{mic}}, \quad (47)$$

where e_{mac} , e_{mod} , e_{mic} are the macro error, the modeling error, and the micro error.

Here, \mathbf{u}^0 is the solution of the homogenized problem, \mathbf{u}^H is the FE-HMM solution, $\mathbf{u}^{0,H}$ is the standard (single-scale) FEM solution that is obtained through exact \mathbb{A}^0 ; and $\tilde{\mathbf{u}}^H$ is the FE-HMM solution obtained through exact micro solutions.

For sufficiently regular problems the following a priori estimates hold in the L^2 -norm, the H^1 -norm and the energy-norm:

$$\|\mathbf{u}^0 - \mathbf{u}^H\|_{L^2(\mathcal{B}_0)} \leq C \left(H^{p+1} + \left(\frac{h}{\epsilon}\right)^{2q} \right) + e_{mod}, \quad (48)$$

$$\|\mathbf{u}^0 - \mathbf{u}^H\|_{H^1(\mathcal{B}_0)} \leq C \left(H^p + \left(\frac{h}{\epsilon}\right)^{2q} \right) + e_{mod}, \quad (49)$$

$$\|\mathbf{u}^0 - \mathbf{u}^H\|_{A(\mathcal{B}_0)} \leq C \left(H^p + \left(\frac{h}{\epsilon}\right)^{2q} \right) + e_{mod}. \quad (50)$$

For e_{mod} in (48)–(50) it holds

$$e_{mod} = \begin{cases} 0 & \text{for periodic coupling with } \delta/\epsilon \in \mathbb{N} \\ C \frac{\epsilon}{\delta} & \text{for Dirichlet coupling with } \delta > \epsilon \end{cases} \quad (51)$$

given that the hypotheses hold, that the elasticity tensor \mathbb{A}^ϵ is periodic on the RVE and, that the micro solution is sufficiently smooth, Jecker and Abdulle [2016].

The modeling error for Dirichlet coupling in (48)–(50) is due to boundary layers E et al. [2005] (Thm. 1.2), Abdulle [2009]. So even for $H \rightarrow 0$ and $h \rightarrow 0$ there is a residual error.

The second terms in the estimates (48)–(50) each represent the micro error which is propagated to the macro scale. Although it is described in terms of h and q , it is measured

by macro quantities, i.e. by \mathbf{u}^H in the L^2 -norm, and by macroscopic stress and strain in the energy-norm. Its order deviation from the micro error as measured on the micro scale is twofold; first, since it is in the L^2 -norm of order $2q$ instead of $q + 1$, second, it is in the H^1 - and energy-norm in the order of $2q$ instead of q and therefore and third, since it coincides for the L^2 -norm with the H^1 -/energy-norm.

The unified estimates covering both the macro error as well as the micro error enable uniform micro-macro (h -/ H -) mesh refinements for optimal convergence order but for minimal computational costs.

macro, micro FEM	L^2 -norm	H^1 -/energy-norm
P^p, P^q	$N_{mic} = (N_{mac})^{(p+1)/2q}$	$N_{mic} = (N_{mac})^{p/2q}$

Table 1: Optimal uniform micro-macro refinement strategies: full order for minimal effort. N_{mic} denotes the number of unknowns on the microscale, N_{mac} on the macroscale.

Table 1 displays the optimal uniform micro-macro refinement strategies for the error in the L^2 -norm and the H^1 -/energy-norm. Of course, the strategies' dependency on the polynomial orders of the macro and micro shape functions p and q rely on full regularity of the corresponding BVPs. In the present context of nonlinear homogenization, the additional question arises, whether the estimates apply at all. For that aim we measure the convergence and compare it with the fully linear case in order to properly identify the source of possible order reductions.

5 Novel Algorithmic Solution Concept

5.1 The standard: nested loops

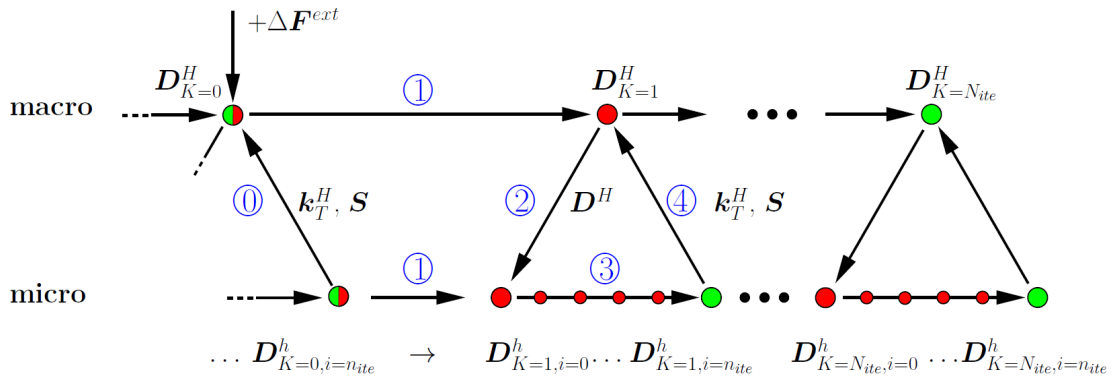


Figure 3: The conventional staggered scheme based on nested, macro-micro solution loops for the nonlinear homogenization by a two-level FEM. Green (red) circles indicate stages (not) in equilibrium.

The algorithmic standard of nonlinear FE² is a staggered solution scheme in terms of a nested loop⁴ embedding the complete solution of the micro problem into one macro solution iteration step as displayed in pseudo-code "Algorithm 1" in Sec. 1. The scheme is typically realized by a nested two-level Newton method.

⁴In Feyel and Chaboche [2000], p.313, referred to as "interleaved finite element algorithms"

This approach is depicted for a Lagrangean formulation in Fig. 3 and goes like this; a loading increment –here in terms of an external force increment $\Delta \mathbf{F}^{ext}$ – shifts both the macro scale as well as the micro scale out of balance of linear momentum, the lights go from green to red. For the solution of the macro problem, the current states of macro stiffness \mathbf{k}_T^H and stress \mathbf{S} are computed on the micro scale and transferred from micro to macro; it is an initialization for the start of a simulation, or an update for the continuation of a simulation, in either case denoted by (0) in Fig. 3. The updated macro stiffness and residual –stress enters the internal force vector being part of the residual– enable the first iteration of the macro Newton, indicated by step (1) in Fig. 3 and its resultant macro displacement vector $\mathbf{D}_{K=1}^H$.

In parallel, the converged micro solution $\mathbf{D}_{K=0, i=n_{ite}}^h$ from the finished previous loading step are transferred to provide favorable start values for solving the micro problems by Newton’s method in the current loading step. The micro problems are driven by the macro displacement field –step (2) in Fig. 3– and are solved subject to the chosen energetically consistent BCs. The iterations in the solution of the micro problem are indicated by the counter $i = 0, \dots, n_{ite}$, step (3) in Fig. 3. Despite its finally vanished micro residuals, the obtained micro solution represents a pseudo-equilibrium state⁵ for its non-zero macro residuals.

Based on the obtained micro solution, macro (element) stiffness \mathbf{k}_T^H and stress \mathbf{S} are passed over to the macro level, step (4) in Fig. 3, which completes the cycle of one macro Newton iteration. These cycles are repeated until the macro Newton is converged.

The inherent hierarchy in the standard staggered scheme in that the outer loop for the macro Newton changes only after the inner loop for the micro Newton has finished is partially prescribed by the physical problem itself. The continuation of the macro solution process after one iteration requires the update of stiffness and stress from the micro scale by the nature of two-scale homogenization in the present format. It is, however, not clear, whether the macro Newton requires fully converged micro solutions for continuation.

5.2 The novel: direct alternations

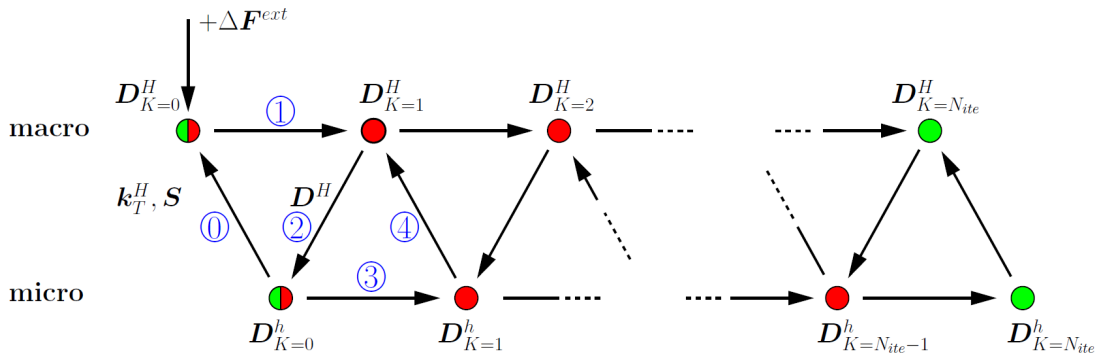


Figure 4: The novel staggered scheme with direct macro-micro alternations in the two-level Newton iterations for the nonlinear homogenization by a two-level FEM. Green (red) circles indicate stages (not) fully converged.

The present work analyzes, whether the nested solution algorithm as described is necessary

⁵They are equally in green color in Fig. 3 even if the macro Newton is not yet converged.

or at least favorable for the homogenization of hyperelastic solids. The criterion is of purely numerical nature, related to convergence in a qualitative and a quantitative manner. The only physical requirement is that at the end of each load step, balance laws are fulfilled both on the micro scale and the macro scale, in terms of the balance of linear momentum in the present context.

We hypothesize that the continuation of the macro Newton does neither require nor take profit in its overall performance from micro solutions that are fully converged. In that case the standard is an expensive luxury.

In line with this hypothesis we advocate an alternative route for a novel staggered scheme as depicted in pseudo-code "Algorithm 2" in Sec. 1 and –applied to the mechanical problem– in Fig. 4, which promises considerable computational savings.

The idea is to replace the embedded-loop solution scheme by a loop of direct micro-macro alternations; after each micro Newton iteration the current stiffness \mathbf{k}_T^H and stress \mathbf{S} are passed over to the macro scale which is followed as in the standard by a macro iteration along with a displacement update for the micro scale.

In the novel version, the number of consecutive iterations on the micro level is restricted to one, hence $i = 0$, the rest $i = 1, \dots, n_{ite}$ of the standard scheme is discarded. In view of the one-to-one alternations one common counter $i = K$ is enough, see Fig. 4. Therefore, a zero residual on the macro scale or the micro scale happens only once, simultaneously at the very end of the loading step.

6 Numerical Examples

In this section the nonlinear FE-HMM is assessed with a focus on two following aspects.

- (A) For the two-level Newton algorithm we compare the standard version with the performance of the proposed version using direct micro-macro alternations.
- (B) Assessment of the a-priori error estimates (48)–(50) for the case of geometrical nonlinearity along with either linear elasticity or (nonlinear) hyperelasticity while keeping in mind that the estimates are proved for linear elasticity in a geometrical linear frame. A comparison with the convergence of the fully linear case is necessary to identify, whether a deviation from the theoretical order is due to the nonlinearity of the considered problem or due to the reduced regularity of the micro problem setting itself. In either case, the errors are calculated by means of an accurate reference solution ("overkill"-solution) on very fine meshes.

The macro problem common to all micro problems is a bending-dominated cantilever beam. It exhibits length l in x -direction, height h in y -direction, and thickness t in z -direction. It is clamped at $x=0$ and subject to force control by an external line load \mathbf{f} or to displacement control. If not otherwise stated, it holds $l = 5000$ mm, $h = 1000$ mm, $b = 100$ mm. The RVE side length ϵ as well as type and magnitude of loading is defined in each example separately.

For hyperelasticity we consider an isotropic neo-Hookean constitutive law frequently used for rubber-like materials. The free energy function exhibits the form

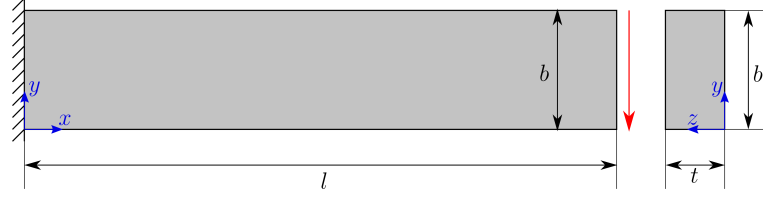


Figure 5: Macroproblem: Cantilever beam, geometry and boundary conditions. For notational convenience we use the Cartesian coordinates (x, y, z) replacing the previous (x_1, x_2, x_3) coordinate system.

$$\psi = \frac{\lambda}{4} (J^2 - 1) - \left(\frac{\lambda}{2} + \mu \right) \ln J + \frac{\mu}{2} (\text{tr } \mathbf{C} - 3), \quad (52)$$

where λ and μ are the Lamé parameters, $J = \det \mathbf{F}$ is the Jacobian and \mathbf{C} is the right Cauchy-Green deformation tensor. From ψ and the hyperelasticity relations for stress and the tangent, $\mathbf{S} = 2\partial_{\mathbf{C}}\psi$, $\mathbb{C} = 4\partial_{\mathbf{C}}^2\mathbf{C}\psi$, we obtain

$$\mathbf{S} = \frac{\lambda}{2} (J^2 - 1) \mathbf{C}^{-1} + \mu (\mathbf{I} - \mathbf{C}^{-1}), \quad (53)$$

$$\mathbb{C}_{ijkl} = [\lambda (J^2 - 1) - 2\mu] \mathbb{A}_{ijkl} + \lambda J^2 C_{ij}^{-1} C_{kl}^{-1}, \quad (54)$$

$$\text{with } \mathbb{A}_{ijkl} = \frac{\partial \mathbf{C}^{-1}}{\partial \mathbf{C}} = -\frac{1}{2} (C_{ik}^{-1} C_{jl}^{-1} + C_{jk}^{-1} C_{il}^{-1}). \quad (55)$$

The considered microstructures consist in either case of two different elastic phases. In view of their considerable differences in morphology, the elasticities of the phases are comprehensively chosen to be same; the material parameters are given in Tab. 2 for linear elasticity and neo-Hookean hyperelasticity.

phase	Linear Elasticity		Neo-Hooke	
	E (N/mm ²)	ν	λ (N/mm ²)	μ (N/mm ²)
1	100 000	0.2	27 777.78	41 666.67
2	40 000	0.2	11 111.11	16 666.67

Table 2: Material parameters for two-phase microstructure.

The simulations are carried out by a C++ code using MPI-parallelization.

6.1 Escher's Pegasus

The first example considers on the macro scale a cantilever beam as displayed in Fig. 5, which is subject at $x = l$ to a lineload of magnitude 200 N/mm in negative y -direction. The material is a periodic, two-phase microstructure as displayed in Fig. 6 similar to the tessellation "Pegasus N°105" of the Dutch graphic artist M.C. Escher (1898-1972). The material's elastic parameters are given in Tab. 2

6.1.1 Micro convergence for linear elasticity and Neo-Hookean hyperelasticity

The reference solution for micro convergence analysis is calculated with ndof=24

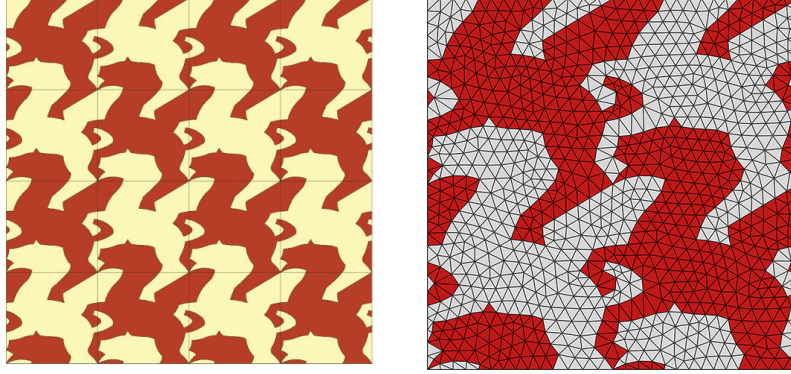


Figure 6: Pegasus: (left) Periodic tessellation with 2×2 unit cells and (right) a triangulation of the unit cell.

on the macro scale domain (5×1 macro elements) and $\text{ndof} = 2\,262\,584$ on the micro scale with $\epsilon = 110$ mm.

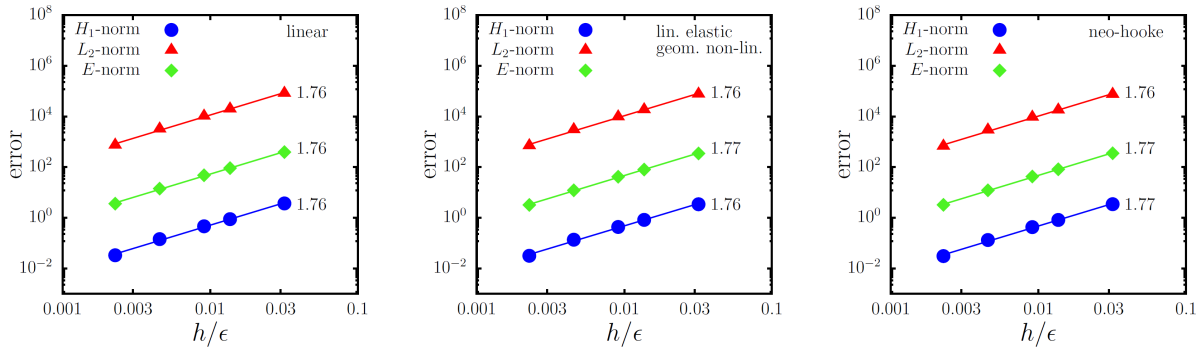


Figure 7: Pegasus: Micro convergence for (left:) fully linear, (middle:) linear elasticity along with geometrical nonlinearity, (right:) Neo-Hookean hyperelasticity.

The convergence diagrams in Fig. 7 indicate that the convergence order in all considered norms is virtually insensitive to the nonlinearities introduced by the kinematics and the hyperelastic constitutive law. The measured convergence orders are below the full theoretical order of $2q = 2$ which is caused by the reduced regularity of the micro problem already visible in the results for the fully linear case.

6.1.2 Standard Newton versus Alternating Newton In order to calculate the speedup factor of the alternating Newton method related to the standard Newton method, the solution for $\text{ndof}_{\text{mac}} = 24$ and $\text{ndof}_{\text{mic}} = 2\,262\,584$ is calculated by both the methods employing 4 loading steps. The corresponding overall performance and computational timing are compared in Table 3.

method	load step	N_{ite}^{mac}	t_{mac}	u_{max}	t_{LS}
standard Newton	1	4	00:07:27	276.8	00:27:09
	2	5	00:08:45	550.7	00:42:31
	3	5	00:08:47	818.1	00:43:53
	4	5	00:08:45	1076.5	00:43:52
alternating Newton	1	5	00:05:08	276.8	00:25:27
	2	5	00:05:09	550.7	00:25:45
	3	5	00:05:10	818.1	00:25:48
	4	5	00:05:09	1076.6	00:25:52
total speedup factor = 1.53					

Table 3: Pegasus: Standard Newton versus alternating Newton where N_{ite}^{mac} is the number of macro iterations, t_{mac} is the compute time for a macro load step, u_{max} is the maximum of the normed nodal displacement vectors and t_{LS} is the compute time for a load step. Compute time has the format (HH:mm:ss) for hours, minutes, and seconds.

Table 3 indicates that the alternating Newton converges properly as indicated by the maximum nodal displacement coinciding with the solution of the standard two-level Newton. Remarkably, in only one out of four loading steps the alternating Newton requires one additional macro Newton iteration for convergence. The overall speedup of 1.53 quantifies the benefit of the alternating Newton.

load step number	macro ite	macro residual	
		standard Newton	alternating Newton
4 (out of 4)	1	1.0000e+00	9.9999e-01
	2	1.4152e+01	1.4114e+01
	3	6.3705e-02	4.7410e-02
	4	4.5369e-04	5.8777e-04
	5	1.8262e-08	6.1250e-06
1 (out of 1)	1	1.0000e+00	1.0000e+00
	2	6.6287e+01	6.6301e+01
	3	4.0499e+00	3.1304e+00
	4	2.3008e-02	1.1509e-02
	5	7.5719e-05	1.4101e-04
	6	5.0931e-09	1.5738e-06

Table 4: Escher’s Pegasus: Comparison of the macro residuals for standard Newton versus alternating Newton in load step 4 (out of 4) and load step 1 (out of 1).

Table 4 compares the convergence of the macro Newton for the two different solution strategies in terms of their macro residuals. Independent of the magnitude of the load step the number of required iterations is the same for both methods, although the alternating Newton exhibits a minor deviation from quadratic convergence in its last iteration.

Table 5 lists the speedup factors of the novel solution strategy for different discretizations; they vary from 1.27 to almost 2.6. Increasing the micro discretization while keeping the macro discretization fixed results in a modest increase in the speedup factor. Vice versa,

macro ndof	micro ndof	speedup factor			
		linear elastic		neo-Hooke	
		$N_{LS}=4$	$N_{LS}=1$	$N_{LS}=4$	$N_{LS}=1$
24	1 946	1.50	1.38	1.50	1.27
	11 942	1.40	1.56	1.31	1.28
	25 820	1.44	1.48	1.39	1.29
	101 918	1.44	1.47	1.38	1.31
	384 930	1.48	1.48	1.39	1.30
	2 262 584	1.53	1.56	1.45	1.40
1 122	1946	1.64	1.63	1.35	2.57
4 242		1.66	1.58	1.31	1.80
16 482		1.59	1.59	1.31	1.83
64 962		1.56	1.40	1.33	1.76
257 922		1.57	1.44	1.33	1.70
4 103 682		1.55	1.49	1.31	1.63

Table 5: Escher’s Pegasus: speedup factors of alternating Newton compared to standard Newton depending on discretizations and the type of the employed elastic constitutive law, where N_{LS} is the total number of load steps.

increasing the macro discretization while keeping the micro discretization fixed results in a modest decrease of the speedup factors. The two trends hold –apart from some outliers– for linear elasticity as well as neo-hookean hyperelasticity and they are insensitive to the load step size likewise. For linear elasticity the speedup factor is higher than for neo-Hooke in general, the exception is the case where ndof_{mac} is in the order of or larger than ndof_{mic} ; here the speedup factor for the hyperelastic case is higher, if the load is applied in one single step instead of four.

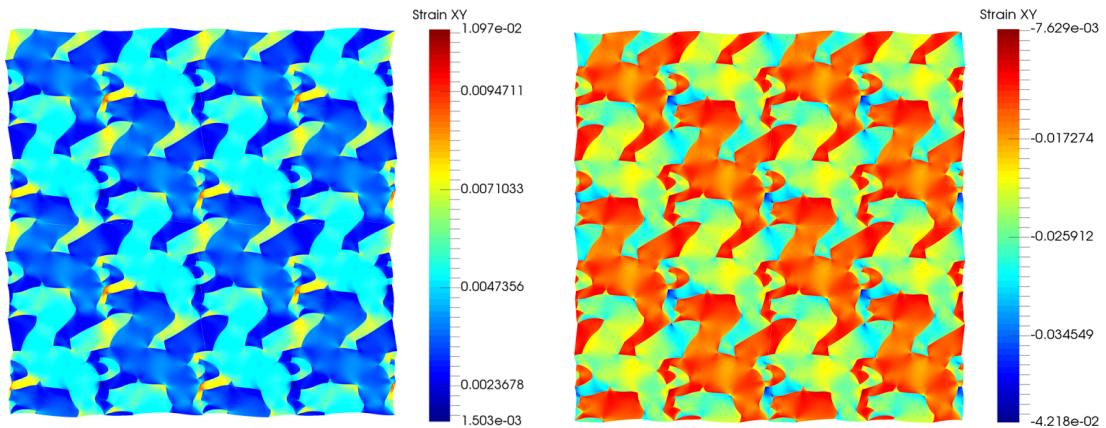


Figure 8: Escher’s Pegasus: contour plot of shear strain component E_{xy} (left) at $x = 3943.37\text{mm}$, $y = 211.32\text{ mm}$ and (right) at $x = 1056.62\text{ mm}$, $y = 788.67\text{ mm}$.

Figure 8 shows the distribution of shear strain $2E_{xy}$ for a 2×2 RVE-array of the Pegasus microstructure with periodic fluctuations at two selected points in the beam.

6.2 Escher’s Swan

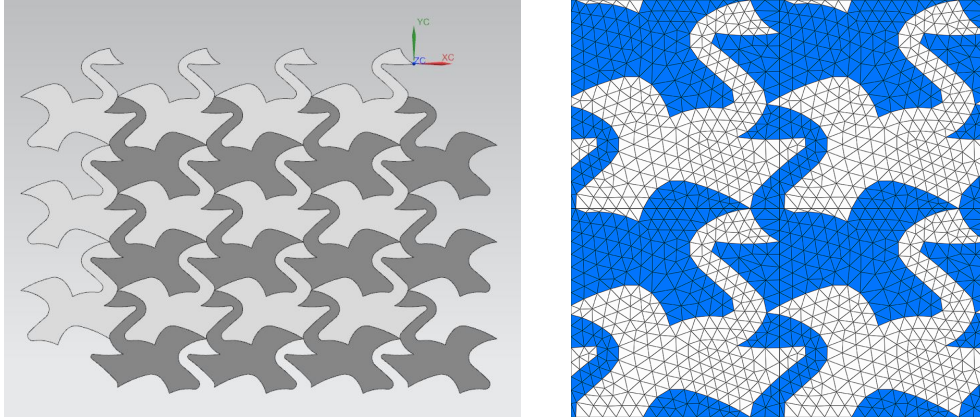


Figure 9: Escher’s Swan: (Left) Periodic tessellation, (right) discretization of a 2×2 unit cells.

In this example a two-phase microstructure is used that follows Escher’s ”Swan N°96” tessellation Fig. 9 (left); each phase follows from each other by reflection and translation. Figure 9 (right) shows a unit cell along with a discretization using linear triangles, hence $q = 1$. In this example phase 1 is assigned to the swan to the left in blue color, and of phase 2 is assigned to the swan to the right in white color. The material parameters for linear elastic and neo-Hookean material laws are given in Tab. 2 of Sec. 6.1.

The macro scale BVP is again the cantilever beam with unaltered dimensions l, h, t which is subject at $x = l$ to a displacement control where the total displacement of 1100 mm is applied in four loading steps.

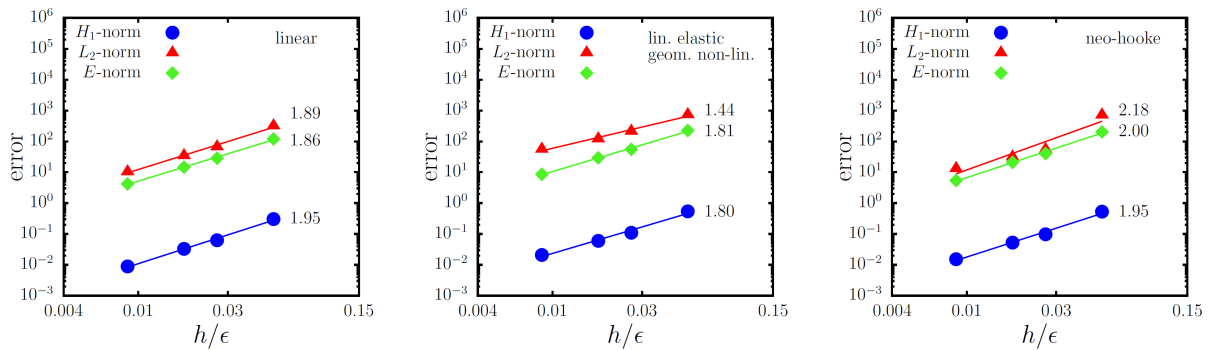


Figure 10: Escher’s Swan: Micro-convergence for (left:) the fully linear case, (middle:) for linear elasticity with geometrical nonlinearity, and (right:) for Neo-Hookean hyperelasticity.

6.2.1 Micro convergence for linear elasticity and neo-Hookean hyperelasticity

The reference solution for the micro convergence analysis is obtained for $\text{ndof}=24$ on the macro domain (5×1 macro elements) and $\text{ndof}=574922$ on micro domains with $\epsilon = 11.4$ mm.

The convergence diagrams for linear elasticity and neo-Hookean material laws are displayed in Fig. 10. Here, the fully linear case achieves almost the full theoretical order in

all norms, $2q = 2$. For the combination of linear elasticity along with geometrical linearity, the convergence order is throughout reduced compared to the fully linear case, most pronounced in the L_2 norm. Remarkably, the convergence order for the fully nonlinear case of neo-Hookean hyperelasticity exhibits excellent convergence rates, in the L_2 norm even above the nominal order 2.0.

method	load step	N_{ite}^{mac}	t_{mac}	u_{max}	t_{LS}
standard Newton	1	4	00:01:54	279.3	00:07:03
	2	4	00:02:12	561.7	00:08:32
	3	4	00:02:12	847.3	00:08:49
	4	4	00:02:16	1136.6	00:08:59
alternating Newton	1	4	00:01:22	279.3	00:05:27
	2	5	00:01:23	561.7	00:06:54
	3	5	00:01:23	847.3	00:06:54
	4	5	00:01:22	1136.6	00:06:53
total speedup factor = 1.28					

Table 6: Escher’s Swan: Standard Newton versus alternating Newton where N_{ite}^{mac} is the number of macro iterations, t_{mac} is the compute time for a macro load step, u_{max} is the maximum of the normed nodal displacement vectors and t_{LS} is the compute time for a load step.

macro ndof	micro ndof	speedup factor		
		linear elastic	neo-Hooke	
24	674	1.25	1.20	
	3 248	1.68	1.05	
	7 222	1.26	1.11	
	27 444	1.25	1.20	
	74 486	1.21	1.18	
	574 922	1.28	1.23	
1 122	674	2.13	1.50	
		4 242	1.53	1.44
		16 482	1.56	1.26
		64 962	1.56	1.37
		257 922	1.76	1.44
		4 103 682	1.63	1.49

Table 7: Escher’s Swan: speedup factors of alternating Newton compared to standard Newton for different discretizations and types of elastic constitutive laws.

6.2.2 Standard Newton versus alternating Newton The overall performance and computational time of the reference solution calculated by standard and alternating Newton method is compared in Tab. 6. We can observe that the maximum nodal displacement units in both the methods are equal and the speedup factor is 1.28. In the present

example the alternating Newton method requires in 3 out of 4 loading steps in each case 5 macro Newton iterations and therefore one more than for the standard nested Newton. A richer picture on the speedup factors of the alternating Newton method for different discretizations is given in Tab. 7. Among the four cases considered in Tab. 7 the case of linear elasticity along with geometrical nonlinearity results for $\text{ndof}_{\text{mac}} \gg \text{ndof}_{\text{mic}}$ in the highest speedup factors, throughout above 1.5.

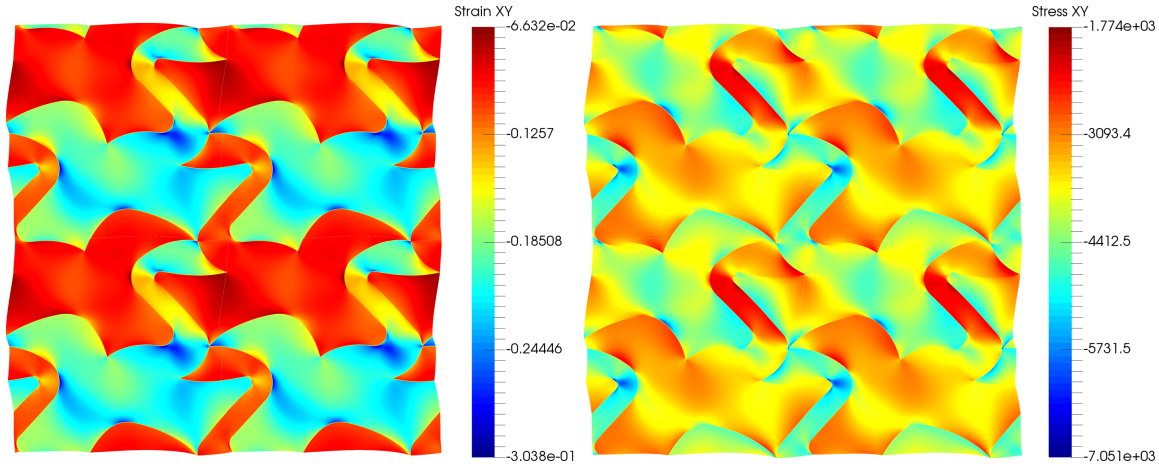


Figure 11: Escher's Swan: at $x = 1056.62$ mm, $y = 788.67$ mm the contour plot (left) of shear strain $2E_{xy}$ and (right) of von-Mises stress S_{xy} .

Figure 11 displays for the macroscopic shear deformation of the quadratic plate; the stiffer phase 1 (swan to the left) shows for its higher stiffness smaller shear strains $2E_{xy}$, in the right the corresponding shear stress is shown S_{xy} .

6.3 DFG-Heisenberg



Figure 12: DFG-Heisenberg: (Left) two-phase distribution, (right) contour plot of shear strain $2E_{xy}$ at position $x = 666.67$ mm, $y = 333.34$ mm.

As an example of pixel-based microstructure representation we consider the two-phase portrait of Werner Heisenberg which serves as the program logo of the German Research Foundation (DFG) as shown in the left of Fig. 12.

The discretization of this image is carried out using pixel to mesh conversion, phases are defined by conversion into binaries according to the pixels' rgb color code. The blue matrix is the softer phase 1, the white Heisenberg inclusion along with DFG initials is the stiffer phase 2, they both exhibit the elasticity properties listed in Tab. 2.

The macro scale BVP is a cantilever beam with, here, length $l = 1000$ mm, $h = 1000$ mm, $b = 100$ mm, which is loaded at $x = l$ by a line load of magnitude 100 N/mm in negative y -direction. PBCs are applied to the micro domains of length $\epsilon = 1$ mm.

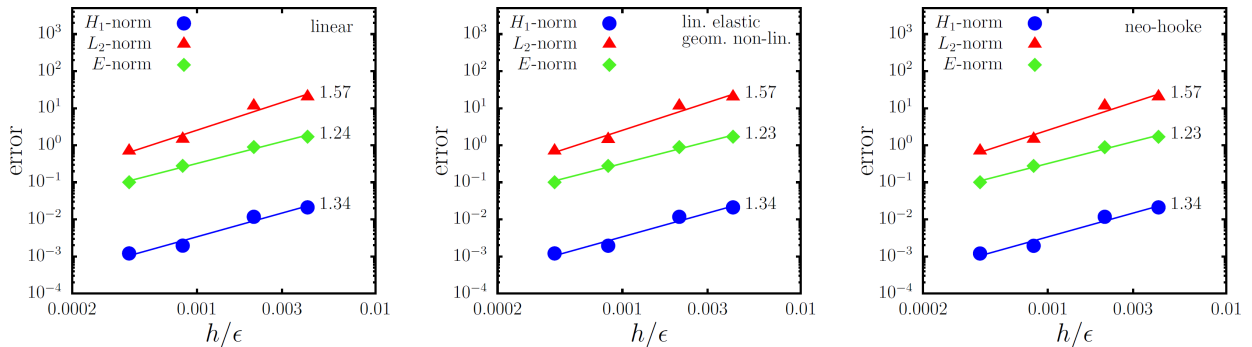


Figure 13: DFG-Heisenberg: Micro-convergence for (left:) the fully linear case, (centre:) for linear elasticity with geometrical nonlinearity, and (right:) for neo-Hookean hyperelasticity.

6.3.1 Micro convergence for linear elasticity and neo-Hookean hyperelasticity

The reference solution for the convergence analysis is obtained by a discretization of $\text{ndof} = 46\,099\,202$ on the micro domain employing a characteristic element width of $h = 1/4800$ mm with $q = 1$. The discretization directly follows from the pixels of the original image. Since we are mostly interested in the micro convergence and differences between the cases having different levels of nonlinearity, a simple driver on the macro scale in terms of one triangular macro element with $p = 1$ is enough.

The measured convergence orders in the diagrams of Fig. 13 are considerably reduced compared to the theoretical order of $2q = 2$; it is most pronounced in the energy norm and least pronounced in the L_2 norm. Due to almost identical results for the fully linear case with the nonlinear cases it can be concluded that the nonlinearities by geometry and hyperelasticity have no impact on convergence.

6.3.2 Standard Newton versus alternating Newton

In order to calculate the speedup factor of the alternating Newton method over standard Newton method, solutions for different micro discretizations are calculated by keeping the macro discretizations constant. The speedup factors are tabulated in Tab. 8.

The speedup is throughout above 1.2 and ranges up to 1.82, such that the novel solution strategy pays off in either case. For a fixed macro discretization the speedup factor increases independent of the elasticity law the finer the micro discretization, which is true apart from some outliers. For the case of a fixed micro discretization the speed-factor is relatively insensitive to the macro discretization. These trends are consistent with the previous example of Escher's Pegasus.

macro ndof	micro ndof	speedup factor	
		linear elastic	neo-Hooke
8	116162	1.41	1.41
	462722	1.37	1.32
	1847042	1.51	1.41
	2884802	1.58	1.49
	11529602	1.82	1.58
	46099202	1.73	1.73
882	116162	1.21	1.38
3362		1.22	1.41
13122		1.22	1.41
51842		1.28	1.41
206082		1.27	1.25

Table 8: DFG-Heisenberg: speedup factors of alternating Newton compared to standard Newton depending on discretizations and type of elastic constitutive law.

6.4 Nanoporous gold

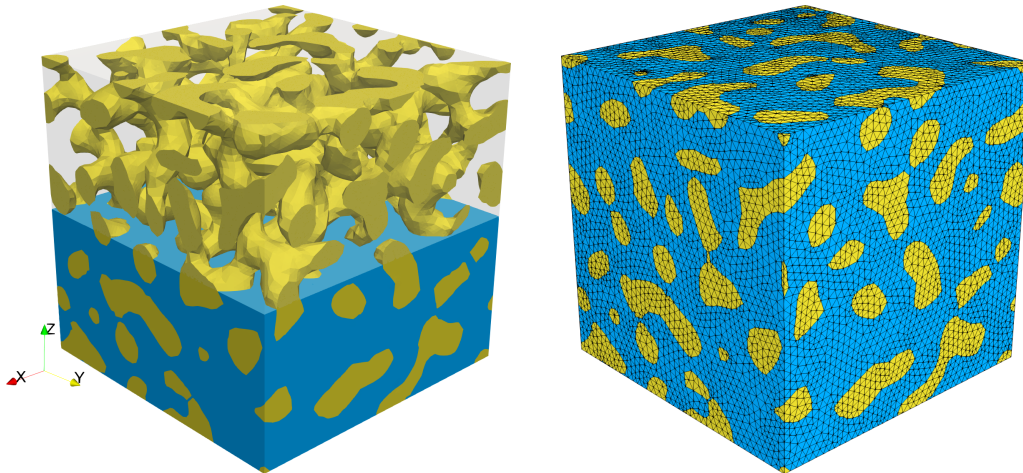


Figure 14: Nanoporous gold composite: (Left) gold phase distribution, (right) discretization with $\text{ndof}=1\,807\,389$.

Nanoporous gold exhibits extraordinary properties such as high catalytic activity Fujita et al. [2012], surface-stress induced macroscopic bending of cantilevers, Kramer et al. [2004] and it is a promising component for gold-polymer nanocomposites Griffiths et al. [2017].

Here we consider a gold-polymer nanocomposites with the nanoporous gold phase embedded in a softer second phase. Linear Dirichlet boundary conditions are applied on the RVE. The Young’s moduli of the gold phase is $E_i = 100\,000\text{ N/mm}^2$ and the matrix phase $E_m = 40\,000\text{ N/mm}^2$ exhibit the contrast of $E_i/E_m = 2.5$, for the Poisson’s ratio it holds $\nu = 0.2$. The volume ratio of the gold phase is $V_i/V_{tot} = 0.36$.

The macro BVP is a cantilever beam with length $l = 5000\text{ mm}$, height $h = 1000\text{ mm}$, and thickness $b = 1000\text{ mm}$. At the free end of the cantilever beam displacement control

is applied, where the total displacement of 200 mm is applied to all nodes at $x = l$ in four loading steps.

6.4.1 Micro convergence for linear elasticity and neo-Hookean hyperelasticity

The reference solution for the convergence study is obtained with $\text{ndof}=72$ on the macro domain ($5 \times 1 \times 1$ hexahedral macro elements) and $\text{ndof}=5\,484\,291$ on the micro domain with $\epsilon = 4.03$ mm.

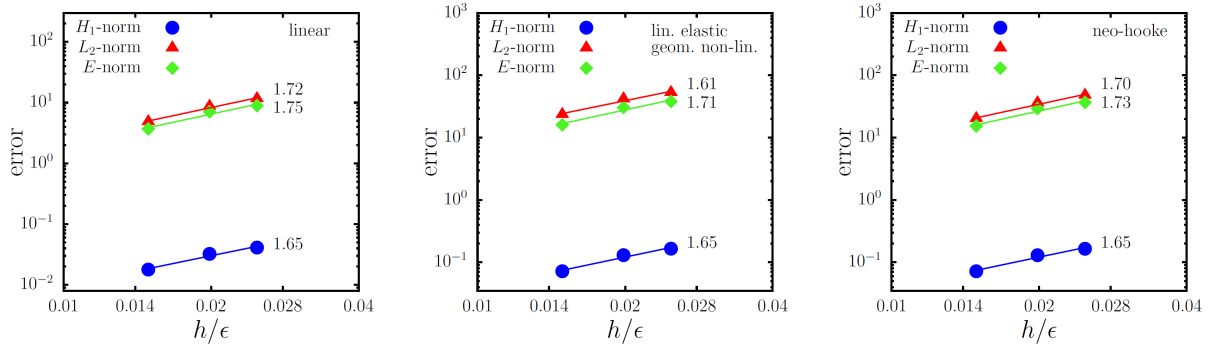


Figure 15: Nanoporous gold composite: Micro-convergence for (left:) the fully linear case, (centre:) linear elasticity with geometrical nonlinearity, and (right:) the case of Neo-Hookean hyperelasticity.

The convergence diagrams are displayed in Fig. 15. The convergence order for the case of geometrical nonlinearity as well as for additional material nonlinearity is virtually the same as for the fully linear case, an exception is the case of geometrical nonlinearity along with linear elasticity in the L_2 norm.

macro ndof	micro ndof	speedup factor	
		linear elastic	neo-Hooke
72	262 308	1.75	1.69
	353 904	1.77	1.71
	690 162	1.98	1.82
	1 518 654	1.88	1.86
	1 807 389	1.86	1.86
297	262 308	1.85	1.85
1575		1.90	1.89
4557		1.78	1.81

Table 9: Nanoporous gold composite: speedup factors of alternating Newton compared to standard Newton depending on discretizations and type of elastic constitutive law.

6.4.2 Standard Newton versus alternating Newton The speedup factors for the alternating Newton are as tabulated in Tab. 9. They range from 1.7 to almost 2 and are higher than in the considered 2d homogenization problems. There is no clear trend in the speedup factors for finer meshes except of for the case of neo-Hookean hyperelasticity, where the speedup increases for an increase of the unknowns on the RVE level. For the

other cases of various discretization (combinations of micro to macro) the speedup is around 1.8 with relatively minor variance.

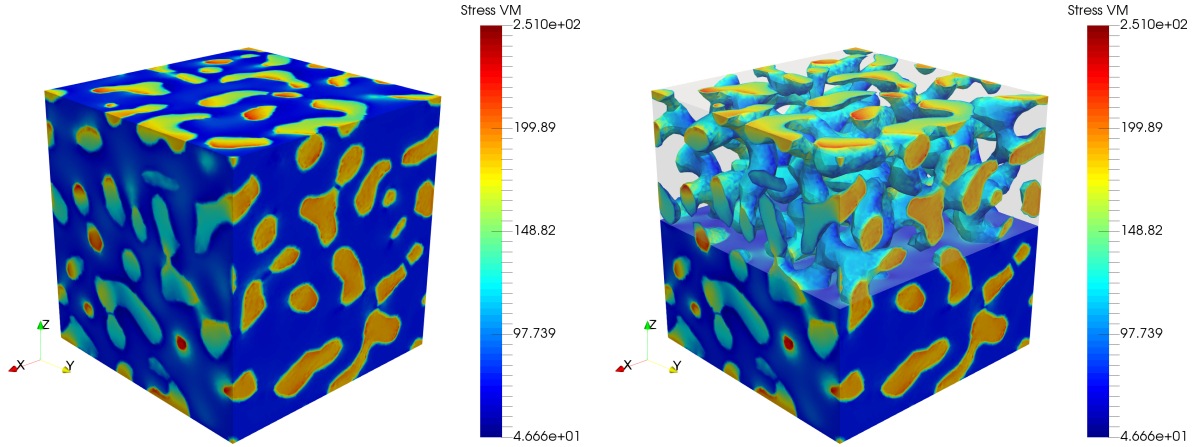


Figure 16: Nanoporous gold composite: von Mises stress distribution in (N/mm²) at $x = y = z = 605.6624$ mm.

7 Summary

The main results of the present paper shall be summarized.

1. The Finite Element Heterogeneous Multiscale Method FE-HMM was developed for geometrical nonlinearity and hyperelastic solids in a Lagrangean setting.
2. Existing a priori estimates for the fully linear case (linear elasticity in a geometrical linear frame) were assessed for the present nonlinear case in numerical tests and confirmed for sufficient regularity of the BVPs. In either case the convergence results in the nonlinear elastic regime are close to those of the fully linear case for the investigated examples.
3. The staggered, micro-macro solution concept in terms of a two-level Newton algorithm was revised and replaced.
 - The standard approach in terms of nested loops can safely and efficiently be replaced by direct alternations between micro and macro solution iterations. The converged solution of the micro problems for each of the macro iterations is neither necessary for achieving convergence nor favorable for the resultant speed.
 - For the considered problems the novel concept (i) is robust with respect to large loading steps (ii) exhibits speedup factors in the range of 1.05 up to 2.57 in 2D, and in the range from 1.69 to 1.98 in 3D, where the speedup is on average higher in 3D than in 2D.
 - The observed minimal speedup is above 1.0, such that the novel concept does not slow down simulations. Since the speedup of 1.0 is clearly not a granted lower bound, monitoring the macro convergence on-the-fly in terms of the required iterations can guarantee negative effects.

- A particular appeal of the proposed concept is its simplicity and ease of implementation.
4. The advantages of the novel concept was demonstrated for FE-HMM simulations. It equally applies for FE² for the equality of the methods despite minor differences in micro-macro stiffness transfer.

It is expected that the novel speedup concept can be used in different applications as e.g. in coupled problems such as electro-/magneto-/mechanical-coupling, or generally, in any other nonlinear problem set where a staggered, two-level algorithmic solution concept in terms of an embedded loop is standard.

Inelastic problems in homogenization require a separate analysis in order to arrive at valid conclusions on the applicability of the proposed speed-up concept, which will be presented elsewhere.

Acknowledgments. Bernhard Eidel acknowledges support by the Deutsche Forschungsgemeinschaft (DFG) within the Heisenberg program (grant no. EI 453/2-1). Simulations were performed with computing resources granted by RWTH Aachen University under project ID prep0005. This has enabled the present work.

References

- A. Abdulle, Analysis of the heterogeneous multiscale FEM for problems in elasticity, *Math. Models Methods Appl. Sci.* 16(4) (2006) 615–635.
- A. Abdulle, The Finite Element Heterogeneous Multiscale Method: a computational strategy for multiscale PDEs, *Math. Sci. Appl.* 31 (2009) 133–181.
- A. Abdulle, M.E. Huber, Error estimates for finite element approximations of nonlinear monotone elliptic problems with application to numerical homogenization, *Numer. Meth. Part. D. E.* 32(3) (2016) 955–969.
- A. Abdulle, W. E., B. Engquist, E. Vanden-Eijnden, The heterogeneous multiscale method, *Acta Numer.* 466 (2012) 1–87.
- G. Allaire, Homogenization and two-scale convergence, *SIAM J. Math. Anal.* 23 (1992) 1482–1518.
- A. Bensoussan, J.L. Lions, G. Papanicolau, *Asymptotic Analysis for Periodic Structures*, North-Holland, Amsterdam (1976).
- D. Cioranescu, P. Donato, *An Introduction to Homogenization*, Oxford University Press, New York (1999).
- N.P. van Dijk, Formulation and implementation of stress-driven and/or strain-driven computational homogenization for finite strain, *Int. J. Numer. Meth. Engng* 107 (2016) 1009–1028.

- W.J. Drugan, J.R. Willis, A micromechanics-based nonlocal constitutive equation and estimates of representative volume element size for elastic composites, *J. Mech. Phys. Solids* 44 (1996) 497–524.
- W. E, B. Engquist, The heterogeneous multi-scale methods, *Commun. Math. Sci.* 1 (2003) 87–132.
- W. E, B. Engquist, X. Li, W. Ren, E. Vanden-Eijnden, Heterogeneous multiscale methods: a review, *Commun. Comput. Phys.* 2 (2007) 367–450.
- W. E, P. Ming, P. Zhang, Analysis of the heterogeneous multi-scale method for elliptic homogenization problems, *J. Amer. Math. Soc.* 18 (2005) 121–156.
- B. Eidel, A. Fischer, The heterogeneous multiscale finite element method FE-HMM for the homogenization of linear elastic solids, *PAMM* 16 (2016) 521–522.
- B. Eidel, A. Fischer, The heterogeneous multiscale finite element method FE-HMM for the homogenization of linear elastic solids and a comparison with the FE² method, *Comput. Methods Appl. Mech. Engrg.* 329 (2018) 332–368.
- B. Eidel, A. Fischer, A. Gote, A nonlinear FEHMM formulation along with a novel algorithmic structure for finite deformation elasticity, *PAMM* 18 (2018) e201800457.
- F. Feyel, J.L. Chaboche, FE² multiscale approach for modelling the elastoviscoplastic behaviour of long fibre SiC/Ti composite materials, *Comput. Methods Appl. Mech. Engrg.* 183 (2000) 309–330.
- F. Feyel, A multilevel finite element method (FE²) to describe the response of highly non-linear structures using generalized continua, *Comput. Methods Appl. Mech. Engrg.* 192 (2003) 3233–3244.
- A. Fischer, B. Eidel, Convergence and error analysis of FE-HMM/FE² for energetically consistent micro-coupling conditions in linear elastic solids, *Eur. J. Mech. A-Solid*, 77 (2019) 103735.
- J. Fish, Q. Yu, K. Shek, Computational damage mechanics for composite materials based on mathematical homogenization, *Int. J. Numer. Meth. Eng.* 45 (1999) 1657–1679.
- T. Fujita, P. Guan, K. McKenna, X. Lang, A. Hirata, L. Zhang, T. Tokunaga, S. Arai, Y. Yamamoto, N. Tanaka, Y. Ishikawa, N. Asao, Y. Yamamoto, J. Erlebacher, and M. Chen, Atomic origins of the high catalytic activity of nanoporous gold, *Nat. Mater.* 11 (2012) 775–780.
- E. Griffiths, S. Bargmann, B.D. Reddy, Elastic behaviour at the nanoscale of innovative composites of nanoporous gold and polymer, *Extreme Mech. Lett.* 17 (2017) 16–23.
- R. Grytz, G. Meschke, Consistent micromacro transitions at large objective strains in curvilinear convective coordinates, *Int. J. Numer. Meth. Engrg.* 73(6) (2008) 805–824.
- J.M. Guedes, N. Kikuchi, Preprocessing and postprocessing for materials based on the homogenization method with adaptive finite element methods, *Comput. Methods Appl. Mech. Engrg.* 83 (1990) 143–198.

-
- P. Henning, M. Ohlberger, Error control and adaptivity for heterogeneous multiscale approximations of nonlinear monotone problems, *Discrete Cont. Dyn.-S* 8(1) (2015) 119–150.
- R. Hill, Elastic properties of reinforced solids: some theoretical principles, *J. Mech. Phys. Solids* 11 (1963) 357–372.
- R. Hill, On constitutive macro-variables for heterogeneous solids at finite strain, *Proc. R. Soc. London, Ser. A* 326 (1972) 131–147.
- A. Javili, Chatzigeorgiou, P. Steinmann, Computational homogenization in magneto-mechanics, *Int. J. Numer. Meth. Eng.* 50(25–26) (2013) 4197–4216.
- O. Jecker, A. Abdulle, Numerical experiments for multiscale problems in linear elasticity, in: B. Karasözen, M. Manguoğlu M., M. Tezer-Sezgin, S. Göktepe, Ö. Uğur (Eds.) *Numerical Mathematics and Advanced Applications ENUMATH 2015. Lecture Notes in Computational Science and Engineering*, vol. 112. Springer, Cham (2016) 123–131.
- A. Klawonn, O. Rheinbach, Robust FETI-DP methods for heterogeneous three dimensional elasticity problems, *Comput. Methods Appl. Mech. Engrg.* 196 (2007) 1400–1414.
- A. Klawonn, O. Rheinbach, Highly scalable parallel domain decomposition methods with an application to biomechanics, *Z. Angew. Math. Mech.* 90(1) (2010) 5–32.
- A. Klawonn, S. Köhler, M. Lanser, O. Rheinbach, Computational homogenization with million-way parallelism using domain decomposition methods, *Comput. Mech.* <https://doi.org/10.1007/s00466-019-01749-5>.
- V. Kouznetsova, W.A.M. Brekelmans, F.P.T. Baaijens, An approach to micro-macro modeling of heterogeneous materials, *Comput. Mech.* 27 (2002) 37–48.
- V. Kouznetsova, M.G.D. Geers, W.A.M. Brekelmans, Multi-scale constitutive modelling of heterogeneous materials with a gradient-enhanced computational homogenization scheme, *Int. J. Numer. Meth. Eng.* 54 (2002) 1235–1260.
- V. Kouznetsova, M.G.D. Geers, W.A.M. Brekelmans, Multi-scale second-order computational homogenization of multi-phase materials: a nested finite element solution strategy, *Comput. Methods Appl. Mech. Engrg.* 193 (2004) 5525–5550.
- D. Kramer, R. N. Viswanath, J. Weissmüller, Surface-stress induced macroscopic bending of nanoporous gold cantilevers, *Nano Lett.* 4(5) (2004) 793–796.
- E. Kröner, *Statistical Continuum Mechanics*, Springer-Verlag, Wien (1971).
- J. Mandel, *Plasticité Classique et Viscoplasticité*, CISM Lecture Notes. Springer-Verlag, Udine, Italy. Wien (1971).
- J.C. Michel, H. Moulinec, P. Suquet, Effective properties of composite materials with periodic microstructure: a computational approach, *Comput. Methods Appl. Mech. Engrg.* 172 (1999) 109–143.

- C. Miehe, J. Schröder, J. Schotte, Computational homogenization analysis in finite plasticity simulation of texture development in polycrystalline materials, *Comput. Methods Appl. Mech. Engrg.* 171 (1999) 387–418.
- C. Miehe, J. Schotte, J. Schröder, Computational micromacro transitions and overall moduli in the analysis of polycrystals at large strains, *Comput. Mat. Sci.* 16 (1-4) (1999) 372–382.
- C. Miehe, A. Koch, Computational micro-to-macro transitions of discretized microstructures undergoing small strain, *Arch. Appl. Mech.* 71 (2002) 300–317.
- C. Miehe, Computational micro-to-macro transitions for discretized micro-structures of heterogeneous materials at finite strains based on the minimization of averaged incremental energy, *Comput. Methods Appl. Mech. Engrg.* 192 (2003) 559–591.
- P. Ming, X. Yue, Numerical methods for multiscale elliptic problems, *J. Comput. Phys.* 214 (2006) 421–445.
- H. Moulinec, P. Suquet, Fast numerical method for computing the linear and nonlinear properties of composites, *CR. Acad. Sci. II* 318 (1994) 1417–1423.
- H. Moulinec, P. Suquet, A numerical method for computing the overall response of nonlinear composites with complex microstructure, *Comput. Methods Appl. Mech. Engrg.* 157 (1998) 69–94.
- M. Ohlberger, A posteriori error estimates for the heterogeneous multiscale finite element method for elliptic homogenization problems, *Multiscale Model. Simul.* 4(1) (2005) 88–114.
- I. Özdemir, W.A.M. Brekelmans, M.G.D. Geers, FE² computational homogenization for the thermo-mechanical analysis of heterogeneous solids, *Comput. Methods Appl. Mech. Engrg.* 198 (2008) 602–613.
- M. Ostoja-Starzewski, Material spatial randomness: from statistical to representative volume element, *Probabilist. Eng. Mech.* 21(2) (2006) 112–132.
- A. Radermacher, S. Reese, POD-based model reduction with empirical interpolation applied to nonlinear elasticity, *Int. J. Numer. Methods Eng.* 107 (2016) 477–495.
- K. Sab, On the homogenization and the simulation of random materials, *Eur. J. Mech. A-Solid* 11(5) (1992) 585–607.
- S. Saeb, P. Steinmann, A. Javili, Aspects of computational homogenization at finite deformations: a unifying review from Reuss’ to Voigt’s bound, *Appl. Mech. Rev.* 68 (2016) 050801.
- E. Sanchez-Palencia, *Non-Homogeneous Media and Vibration Theory*, Lecture Notes in Physics, Vol. 127, Springer, Berlin (1980).
- M. Schneider, F. Ospald, M. Kabel, Computational homogenization of elasticity on a staggered grid, *Int. J. Numer. Meth. Engrg.* 105(9) (2015) 693–720.

-
- M. Schneider, D. Merkert, M. Kabel, FFT-based homogenization for microstructures discretized by linear hexahedral elements, *Int. J. Numer. Meth. Engng.* 109(9) (2017) 1461–1489.
- J. Schröder, A numerical two-scale homogenization scheme: the FE²-method, in: J. Schröder, K. Hackl (Eds.), *Plasticity and Beyond*, CISM International Centre for Mechanical Sciences, (2014) 1–64.
- J. Schröder, D. Balzani, D. Brands, Approximation of random microstructures by periodic statistically similar representative volume elements based on lineal-path functions, *Arch. Appl. Mech.* 81(7) (2010) 975–997.
- R. Shirazi-Nejad, C. Wieners, Parallel inelastic heterogeneous multi-scale simulations. In: Diebels S., Rjasanow S. (eds) *Multi-scale Simulation of Composite Materials*. Mathematical Engineering. Springer, Berlin, Heidelberg, (2019) 57–96.
- D. Soldner, B. Brands, R. Zabihiyan, P. Steinmann, J. Mergheim, A numerical study of different projection-based model reduction techniques applied to computational homogenisation, *Comput. Mech.* 60(4) (2017) 613–625.
- E.A. de Souza Neto, R.A. Feijóo, On the equivalence between spatial and material volume averaging of stress in large strain multi-scale solid constitutive models, *Mech. Mater.* 40 (2008) 803–811.
- I. Temizer, P. Wriggers, On the computation of the macroscopic tangent for multiscale volumetric homogenization problems, *Comput. Methods Appl. Mech. Engrg.* 198(3) (2008) 495–510.
- J. Yvonnet, Q.C. He, The reduced model multiscale method (R3M) for the non-linear homogenization of hyperelastic media at finite strains, *J. Comput. Phys.* 223 (1) (2007) 341–368.
- R. Zeller, P.H. Dederichs, Elastic constants of polycrystals, *Phys. Status Solidi B* 55(2) (1973) 831–842.